PL-TR-94-2086
Physical Sciences Research Papers, No. 670

THERMOCHEMICAL IR SOURCES: COCHISE AND FACELIF EXPERIMENTS

S. M. Miller
W. A. Blumberg
W. T. Rawlins
M. E. Fraser
C. P. Fell
J. I. Steinfeld

14 March 1994

APPROVED FOR PUBLIC RELEASE; DISTRIBUTION UNLIMITED

PHILLIPS LABORATORY
Directorate of Geophysics
AIR FORCE MATERIEL COMMAND
HANSCOM AIR FORCE BASE, MA 01731-3010

"This technical report has been reviewed and is approved for publication"

(Signature)
William A.M. Blumberg, Branch Chief
Simulations Branch
Optical Environment Division

(Signature)
ROGER A. VAN TASSEL, DIRECTOR
Optical Environment Division

This report has been reviewed by the ESC Public Affairs Office (PA) and is releasable to the National Technical Information Service (NTIS).

Qualified requestors may obtain additional copies from the Defense Technical Information Center (DTIC). All others should apply to the National Technical Information Service (NTIS).

If your address has changed, if you wish to be removed from the mailing list, or if the addressee is no longer employed by your organization, please notify PL/TSI, 29 Randolph Road, Hanscom AFB, MA 01731-3010. This will assist us in maintaining a current mailing list.

Do not return copies of this report unless contractual obligations or notices on specific document requires it to be returned.

REPORT DOCUMENTATION PAGE

Form Approved
OMB No. 0704-0188

1. AGENCY USE ONLY (Leave blank)	2. REPORT DATE	3. REPORT TYPE AND DATES COVERED
	14 March 1994	Scientific Final

4. TITLE AND SUBTITLE
Thermochemical IR Sources:
COCHISE and FACELIF Experiments

5. FUNDING NUMBERS
PE: 61102F
PR: 2310/2303
TA: G4/GD
WU: 24/01

6. AUTHOR(S)
S. M. Miller
W. A. Blumberg
W. T. Rawlins*
M. E. Fraser*
C. P. Fell+
J. I. Steinfeld+

7. PERFORMING ORGANIZATION NAME(S) AND ADDRESS(ES)
Phillips Laboratory(GPOS)
29 Randolph Road
Hanscom AFB, MA 01731-3010

8. PERFORMING ORGANIZATION REPORT NUMBER
PL-TR-94-2086
PSRP, No. 670

9. SPONSORING/MONITORING AGENCY NAME(S) AND ADDRESS(ES)

10. SPONSORING/MONITORING AGENCY REPORT NUMBER

11. SUPPLEMENTARY NOTES
* Physical Sciences Inc., 20 New England Business Center, Andover, MA 01810
+ Massachusetts Institute of Technology, Cambridge, MA 02139

12a. DISTRIBUTION/AVAILABILITY STATEMENT
Approved for Public Release
Distribution Unlimited

12b. DISTRIBUTION CODE

13. ABSTRACT *(Maximum 200 words)*
Each of the experiments performed in the COCHISE facility has measured a fundamental chemical quantity such as a relative branching ratio, a quenching rate coefficient, or developed a new detection technique. These measurements are then provided for incorporation into the various atmospheric radiation codes, such as NORSE and SHARC, where they provide a solid experimental footing for modeling the complex chemical system of the upper atmosphere. The following papers provide the details of these experiments.

(a) Branching Ratios for Infrared Vibrational Emission from NO($X^2\Pi$,v'=2-13)
(b) Ro-vibrational Excitation of Carbon Monoxide by Energy Transfer from Metastable Nitrogen
(c) Quenching of N(^{2}D) by O(^{3}P)
(d) Detection of N(^{4}S) by Resonantly Enhanced Multi-photon Ionization Spectroscopy

14. SUBJECT TERMS
COCHISE, FACELIF, Chemiluminescence, Ro-vibrational Excitation
Multi-photon Ionization, NO, CO, N(^{2}D), O, N(^{4}S), Quenching

15. NUMBER OF PAGES
40

16. PRICE CODE

17. SECURITY CLASSIFICATION OF REPORT	18. SECURITY CLASSIFICATION OF THIS PAGE	19. SECURITY CLASSIFICATION OF ABSTRACT	20. LIMITATION OF ABSTRACT
UNCLASSIFIED	UNCLASSIFIED	UNCLASSIFIED	UNLIMITED

CONTENTS

Reprinted from

THE JOURNAL

OF

CHEMICAL PHYSICS

VOLUME 92 NUMBER 3

1 FEBRUARY 1990

Rovibrational excitation of carbon monoxide by energy transfer from metastable nitrogen

MARK E. FRASER AND WILSON T. RAWLINS

Physical Sciences Inc., 20 New England Business Center, Andover, Massachusetts 01810

STEVEN M. MILLER

Air Force Geophysics Laboratory/OPI, Hanscom AFB, Massachusetts 01731

pp. 1758-1767

Published by the

AMERICAN INSTITUTE OF PHYSICS

Rovibrational excitation of carbon monoxide by energy transfer from metastable nitrogen

Mark E. Fraser and Wilson T. Rawlins
Physical Sciences Inc., 20 New England Business Center, Andover, Massachusetts 01810

Steven M. Miller
Air Force Geophysics Laboratory/OPI, Hanscom AFB, Massachusetts 01731

(Received 14 April 1989; accepted 25 October 1989)

The CO fundamental vibration–rotation spectra resulting from the interaction of discharged nitrogen with carbon monoxide at low pressure ($\sim$3 mTorr) exhibit bimodal rotational distributions. We have identified 14 vibrational levels of a rotationally relaxed (80 K) component and eight vibrational levels from a rotationally excited component. The eight rotationally excited bands are best reproduced by a statistical distribution $E = E_R + E_V = 3.7$ eV, which provides sufficient population in the region of the Fortrat reversal ($J \sim 90$) to account for the observed R-branch bandhead formation. The rotationally relaxed vibrational levels are populated by single- and two-quantum transfer from $N_2(v)$, $N_2(v) + CO \rightarrow N_2(v-1,2) + CO(v=1,2)$, and radiative cascade from $CO(A)$ produced by quenching of $N_2(a')$, $N_2(a'\,^1\Sigma_u^-) + CO \rightarrow N_2(X,v) + CO(A\,^1\Pi) \rightarrow CO(v \leq 9) + h\nu$, and relaxation of the rotationally excited component. Kinetic and energetic arguments indicate that a branch of $N_2(a')$ quenching $N_2(a'\,^1\Sigma_u^-) + CO \rightarrow N_2(X,v) + CO(v \leq 14, J)$ is responsible for the rotationally excited component. Surprisal analysis indicates two dynamic mechanisms are responsible for the rotationally excited component. We have modeled the vibrational distribution of the rotationally excited component with equal contributions from a statistical (all v) process and a process favoring excitation of low vibrational levels ($v \leq 4$).

INTRODUCTION

Modest energy depositions (typically < 1 eV) in CO internal states have been observed in photochemical and abstraction reactions. In general, large fractions of the energy above threshold are manifested in product internal states. For example, photolysis of OCS at 157 nm,[1] acetone[2] at 193 nm, and H_2CO[3,4] produces vibrationlly excited CO with rotational excitations up to 0.9 eV. Studies of energy partitioning in CO from the reaction of hot H atoms with CO_2 indicates nearly 1.0 eV in CO internal states[5] with the rotational distribution in the $v = 0$ level following a statistical model.

Greater energy depositions are observed for energy transfer reactions since these interactions have little or no threshold energy. Quenching by $O(2\,^1D)$,[6] $Na(3\,^2P)$,[7,8] $I(5\,^2P_{1/2})$,[9] and $Br(4\,^2P_{1/2})$,[9] and $Hg(6\,^3P_1$ and $6\,^3P_0)$[10] have been observed to produce vibrationally excited CO. Rotational excitations up to 0.8 eV have been reported for the $Na(3\,^2P) + CO$ quenching reaction,[8] which accounts for a large fraction of the total 2.1 eV exoergicity.

The excitation process responsible for the CO excitation reported in this paper is energy transfer from a metastable state of nitrogen. Energy transfer to CO from discharged nitrogen has been examined closely, particularly with respect to the N_2–CO laser.[11,12] High CO vibrational excitation is produced from near-resonant $N_2(v)$ energy transfer and subsequent $CO(v)$ collisional up pumping[13,14] [reactions (1a) and (1b)]

$$N_2(v) + CO(v') \rightarrow N_2(v-1) + CO(v'+1), \quad (1a)$$

$$CO(v) + CO(v') \rightarrow CO(v-1) + CO(v'+1). \quad (1b)$$

Although high CO vibrational levels are produced in this manner, no rotational excitation is observed, which is consistent with the small energy defect for the near-resonant process.

The energy defect from $N_2(a\,^1\Pi)$ quenching[15]

$$N_2(a\,^1\Pi) + CO \rightarrow N_2(X,v) + CO(A\,^1\Pi, v', J') \quad (2)$$

has been determined to be largely manifested in rotation, but the total energy defect is small (< 1000 cm^{-1}), much less than the rotational excitations observed here. The quenching of $N_2(A\,^3\Sigma_u^+)$ by CO[16] produces $CO(a\,^3\Pi)$ with no reported observations of a $CO(v,J)$ product channel.

The energy transfer process reported here represents a previously unobserved quenching reaction of CO with metastable nitrogen. We will show that consideration of kinetic and energetic constraints identifies $N_2(a'\,^1\Sigma_u^-)$ as the responsible agent. We will also present and discuss the results of surprisal analysis of the observed vibrational distributions which indicates the rotationally excited component to be formed by two distinct mechanisms.

EXPERIMENTS

These experiments were performed in the COCHISE (COld CHemiexcitation Infrared Stimulation Experiment) cryogenic discharge afterglow apparatus which is described in detail elsewhere.[17] Excitation of nitrogen is achieved with four parallel microwave discharges (2450 MHz, 50 W) of flowing N_2/Ar mixtures at $\sim$1 Torr total pressure. A diagram of the reaction chamber is shown in Fig. 1. After exiting the discharge tubes, the gas expands into a low pressure ($\sim$3 mTorr), cryogenically pumped chamber ($\sim$20 K), where the molecules enter the collimated field of view of a

 0021-9606/90/031758-10$03.00

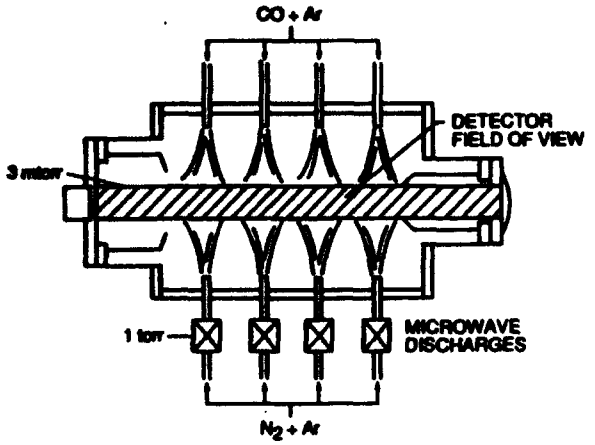

FIG. 1. Diagram of the COCHISE reaction chamber. The physical dimensions of the cell are 0.6 m in length and 0.4 m in diameter.

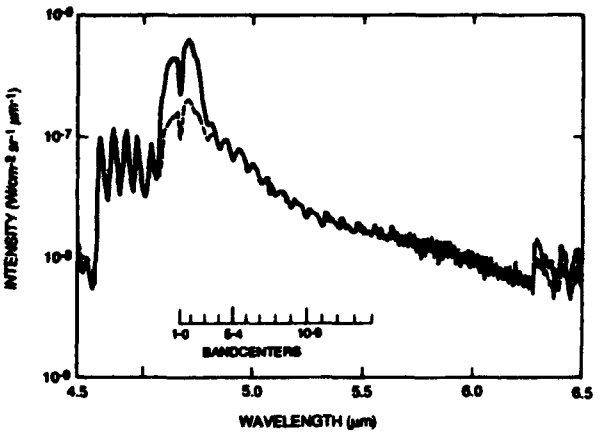

FIG. 2. Data comparison. The solid line shows a typical spectrum obtained under conditions of 12% discharged N_2/Ar reacting with a counterflow of 33% CO/Ar. The dashed line shows data taken at 3.17% N_2/Ar with identical counterflow conditions. Shown below are the band centers for all of the observed transitions.

scanning monochromator/infrared detector assembly. Residence times in the discharge tubes are on the order of 3 to 5 ms; an average time of flight of 0.5 ± 0.1 ms is required for the gases to exit the discharge tubes and enter the field of view. Opposing flows of argon/carbon monoxide are used to create a quasistatic interaction region along the centerline of the field of view, resulting in partial rethermalization of the expansion cooled rotational distributions. The gas residence time in the field of view is ~ 0.3 ms. Gaseous helium refrigerant maintains all internal temperatures at 20 K, excepting the gas lines and optics which are maintained by resistive heating elements at 80 and 40 K, respectively. The temperature of the bath gas in the reaction cell is therefore 80 K.

The infrared emissions are observed by a cryogenic 0.5 m Czerny–Turner monochromator equipped with a liquid-helium-cooled arsenic-doped silicon detector and a grating blazed at 3 μm. A chopper located in front of the monochromator entrance slit modulates the signal at 23 Hz. Data collection is performed with a computer-interfaced lock-in amplifier. The absolute uncertainty in the wavelengths (due to monochromator drive error) of the data is ± 0.003 μm. The data were corrected for instrument responsivity using blackbody calibration spectra taken in the 300–370 K range. The absolute uncertainty in the accuracy of the blackbody temperature is ± 3 K, which results in a relative error of $\pm 14\%$ for 4.0/6.0 μm intensity ratios. Spectra were taken for N_2/Ar mixtures with N_2 mole fractions of 0.005 to 0.12, with a mass-balanced counterflow of CO/Ar with CO mole fractions of 0.018 to 0.35. The data were taken at a spectral resolution typically of 0.013 μm [full width at half-maximum (FWHM)].

RESULTS

In all, 24 emission spectra of the CO fundamental region were obtained at various N_2 and CO mole fractions. The conditions are similar to those in which nitric oxide chemiluminescence was examined.[18] The general features of the emissions are relatively invariant with CO mole fraction, but the intensity of the CO(1–0) emission exhibits a strong N_2 mole fraction dependence as shown in Fig. 2. The relative intensity of the CO(1–0) band changes by a factor of 4 for a factor of 4 change in the N_2 mole fraction.

The envelope degrading to the red of the CO(1–0) band center at 4.666 μm is due to the $\Delta v = 1$ progression from $v \leq 14$. The five sharp red-degraded features to the blue of the CO(1–0) band center, which have a spacing of 29.2 ± 1.4 cm^{-1}, cannot be attributed to CO vibrational emission with a rotational distribution the same as the bath gas (80 K). These bands have not been previously observed in published spectra of CO fundamental emission taken at higher pressures (> 1 Torr).[19–21] At low pressure with the COCHISE apparatus, these features are observed under all conditions that produce the CO fundamental emission. They exhibit no additional structure even at the highest resolution employed (0.0067 μm). Under low nitrogen mole fraction conditions, in which the CO(1–0) emission intensity is greatly reduced, eight bands are observed with three progressing into the CO($\Delta v = 1$) envelope. This is a lower limit considering the overlap of the features to the red of 4.6 μm.

These emissions are not observed in the absence of nitrogen in the discharge mixture. Thus, argon metastables and residual ions do not contribute to the excitation. These features do not correspond to CN(v), electronic N_2 transitions, or NCO. The spectral shape of these features, sharply peaked and degraded to the red, is similar to the nitric oxide R-branch bandheads identified in spectra of chemiluminescence produced from the reaction of discharged nitrogen with oxygen.[18] CO forms bandheads similarly; at sufficiently high rotational excitation, bandheads will form in the R branches and the P branches will extend to the red and do not form bandheads. We have used a spectral generation technique to predict the band shapes and positions of the CO R-branch bandheads. The methodology and results will be presented in detail in the following section. Using this technique the sharp red-degraded features have been positively identified as CO R-branch bandheads. These features are sufficiently intense that we have been able to determine an optimum rotational distribution. Additionally, the P

branches of the rotationally excited component associated with the R-branch bandheads are identifiable. This verifies the spectral assignment and confirms the appropriate choice of rotational distribution.

SPECTRAL ANALYSIS

The data have been analyzed using a spectral generation linear least-squares fitting technique.[22] A computed infinite resolution spectrum is convolved with the instrument scan function (in this case, a symmetric triangle with full width at half-maximum as the spectral resolution) to create simulated spectra for each vibrational transition. The simulated spectra are then fit to each experimental spectrum using a linear least-squares method yielding a determination of the product of the upper state density and the spontaneous emission coefficient of the transition $N_{v'}A_{v',v''}$.

The spectroscopic data used in this study are from Huber and Herzberg.[23] These data were sufficient to reproduce the line positions of both the rotationally relaxed emission features and the R-branch bandheads adequately.

The rotational temperature used to reproduce the CO vibrational progression to the red of 4.6 μm was determined empirically by reproducing the observed branch structure. The optimum temperature was determined to be 80 K, which is the same temperature as the bath gas. Thus, this emission system is rotationally thermalized. The rotational distribution was treated by a simple Boltzmann expression, so that band-integrated vibrational number densities and transition probabilities were used. The transition probabilities were calculated using the dipole moment function of Chackerian *et al.*[24] Fourteen vibrational levels of 80 K CO emission have been positively identified from the data. This corresponds to vibrational excitation of 3.425 eV.

The band-averaged transition probabilities used for the rotationally excited component are the same as those for the 80 K CO emission. We believe these values to be accurate since the CO ground state is $^1\Sigma$ and therefore not subject to spin uncoupling at high J' as discussed for NO.[18] Thus, Hönl–London scaling of the band-averaged transition probabilities should be sufficient to determine the populations of the rotationally excited component accurately.

The 0.013 μm resolution (5 cm^{-1} at 5.0 μm) of the spectral data is insufficient for rotational resolution of the R-branch bandheads so the chosen rotational distributions are those which best reproduce the band shapes and peak positions. To fit the R-branch bandhead features adequately using a Boltzmann distribution requires temperatures of approximately 20 000 K. Although the fits to the lower vibrational levels are adequate, higher vibrational levels are poorly fit and are better described by lower Boltzmann rotational temperatures. This is evidence for an anticorrelation between rotational and vibrational excitations; i.e., the lowest vibrational levels contain the most rotational excitation. Such anticorrelations have been observed in photolysis experiments, abstraction reactions, and energy transfer processes.[1–6,8] In these instances, the observed rotational distributions are sometimes best described by a statistical model.[5] Such a model distributes the population statistically over all accessible states. The model that incorporates the observed anticorrelation between vibrational and rotational excitation is given by

$$P_v^0(J) \propto (2J+1)\{(E_T - E_v) - E_J\}^{1/2}, \quad (3)$$

where E_T is the total energy available for product states, E_v is the vibrational energy, and E_J is the energy of the particular rotational level. Figure 3 contrasts the relative population distributions predicted by Boltzmann and statistical models. The statistical model contains greater relative population in the higher rotational levels at the expense of the lower. Thus, rotational bandhead formation, which requires significant population of rotational levels in the region of the Fortrat parabola vertex ($J_{\text{vertex}} = 92$ for $v = 1$), is readily facilitated by a statistical distribution.

We have examined several values of E_T to determine which best reproduces the positions and spectral shapes of the observed eight bandheads. Values of E_T below 3.0 eV reproduce the lower vibrational levels well, but the predicted bandheads at higher vibrational levels are broadened and red shifted. The responsible mechanism may be seen from Fig. 3. At higher E_v, and lower E_J, the relative population of the rotational levels near the region of the reversal decreases which causes the observed effects. Values of E_T greater than 4.0 eV predict bandhead formation for vibrational levels of ten or greater, which have not been unambiguously identified in the data. We prefer a value of E_T between these two bounds. Comparing fits using several values within this range, we have determined $E_T = 3.7$ eV to be optimum. Values within $\pm$ 0.2 eV of the optimum value produce adequate fits with only small differences.

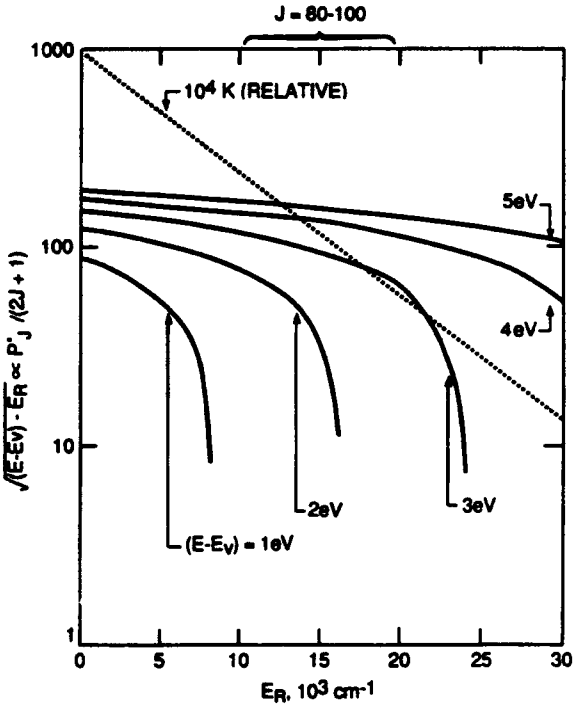

FIG. 3. Comparison of various rotational distributions. Shown are the relative rotational distributions for a 10^4 K Boltzmann and several statistical distributions.

TABLE I. Energetics of CO bandhead formation $E_T = 3.70$ eV.

Vibrational level	E_v(eV)[a]	$E_T - E_v$	J_{vertex}	$E_{J_{vertex}}$(eV)	J_{max}[b]
1	0.266	3.434	92	1.966	123
2	0.528	3.172	91	1.907	118
3	0.788	2.912	90	1.848	114
4	1.044	2.656	90	1.831	109
5	1.296	2.404	89	1.774	104
6	1.546	2.154	88	1.719	98
7	1.792	1.908	87	1.665	93
8	2.035	1.665	87	1.648	87
9	2.274	1.426	86	1.600	81
10	2.511	1.189	85	1.544	74
11	2.744	0.956	84	1.444	66
12	2.974	0.726	84	1.478	58
13	3.201	0.499	83	1.430	48
14	3.425	0.275	82	1.382	35

[a] $E_{CO(v=0)} = 0$.
[b] Calculated from the value for $E_T - E_v$.

Table I shows the energetics of CO bandhead formation for E_T of 3.7 eV. Shown are the values for E_R, $(E_T - E_v)$, the rotational level corresponding to the vertex of the Fortrat parabola, the rotational energy corresponding to this value of J, and the maximum rotational level allowable from E_R.

Figure 4 shows a typical fit to the data using 14 vibrational levels of 80 K CO emission and eight vibrational levels with a statistical rotational distribution corresponding to $E_T = 3.7$ eV. All of the principal spectral features are accurately reproduced. The only features not entirely reproduced fall within the 5.7–6.5 μm region. Figure 5 shows an enlarged view of this region from Fig. 4. The fit is shown by the heavy line. The spacing of the bands shown in Fig. 5 is ~ 6 cm^{-1}. These features have been observed in all spectra containing sufficient intensity in this wavelength region. The fit shows excellent reproduction of the spectral shapes, but does not match the absolute intensity. Figure 4 shows that the 80 K CO emission does not contribute to this spectral region; the discrete features are reproduced by the P branches of the rotationally excited component. Inclusion of $v > 8$ of the rotationally excited component improves the fits in this wavelength region. Due to overlap with the CO envelope, however, unique determination of the populations is not possible, so we have generally excluded these bands from the fits. By comparing fits with different vibrational contributions to the rotationally excited component, we have determined that the majority of the intensity in the 5.7–6.5 μm region arises from the higher vibrational levels ($v' = 6$–8). The relative line spacings may be calculated (omitting $D_{v'}$ correction) from

$$\Delta\nu = P(J) - P(J+1) = (B_{v'} + B_{v''}) - (B_{v'} - B_{v''})(2J+1). \quad (4)$$

For $v' = 6$–8 this wavelength region contains P-branch line spacings of ~ 6 cm^{-1} for rotational levels 50–80. The $N_2(W\,^3\Delta_u, v' = 1 \rightarrow B\,^3\Pi_g, v'' = 0)$ emission in the 6.3–6.6 μm region, which we have previously examined and reported,[22] and signal-to-noise considerations impede determination of the full extent of the P-branch structure. The reproduction of these features, however, by fits to the rotationally excited component confirms the identification of the CO R-branch bandheads.

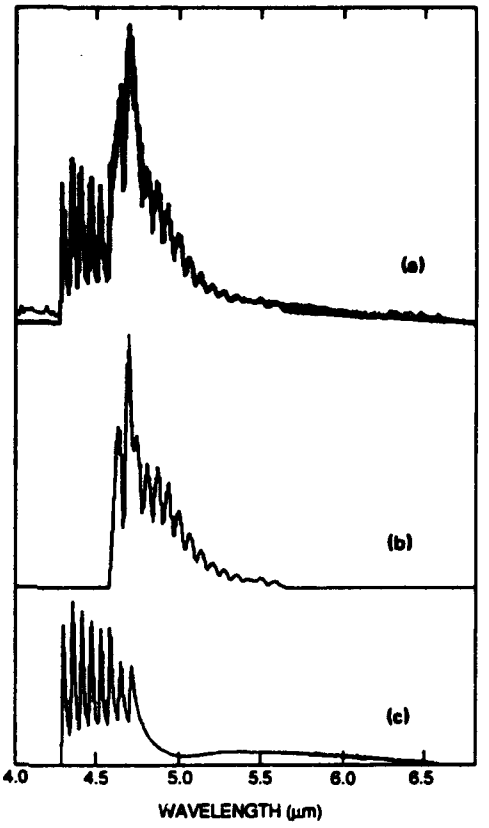

FIG. 4. Data (light line) and best fit (dark line) (a) to 80 K CO fundamental emission ($v' = 1$–14) and CO rotationally excited bands using a statistical distribution with $E_t = 3.7$ eV. The data are the same as used for the dashed line in Fig. 2. The spectral resolution is 0.013 μm. The 80 K CO and rotationally excited simulated spectra which comprise the best fit in (a) are shown in (b) and (c), respectively.

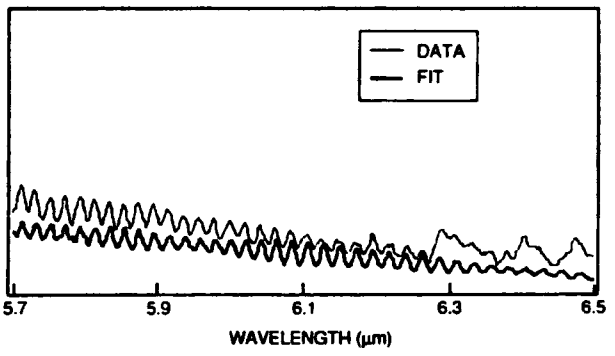

FIG. 5. Enlarged view of the 5.7 to 6.5 μm region of Fig. 4. The data is shown by a light line, the fit by a dark line. The data shown here exhibit a small wavelength offset from the fit well within the monochromator drive error.

All 24 spectra have been fit using 14 80 K CO emission bands and eight vibrational levels of the rotationally excited component, as shown in Fig. 4. The statistical rotational distributions employed in these fits provide a better reproduction of the data, both in the R-branch spectral band shapes and the absolute intensity of the P branches, than do Boltzmann rotational distributions. We consider the statistical model employed here to be a more accurate representation of the true rotational distributions, but it cannot be considered to be a unique determination. Signal-to-noise considerations and band overlap do not permit unambiguous identification of the vibrational-level dependent rotational distributions. The true distributions may deviate from a purely statistical model, possibly containing some Gaussian character. However, the model employed here has successfully demonstrated an anticorrelation between vibrational and rotational excitation and permitted a bound of ~ 3.7 eV to be estimated for the rotationally excited component. Determination of this bound and its similarity to the maximum vibrational excitation of the 80 K CO component 3.425 eV suggests that these two components arise from the same excitation process.

KINETIC INTERPRETATIONS

The kinetics of processes occurring in the COCHISE reaction chamber have been described previously.[18] Owing to the low number densities in the reaction zone, the short residence time in the field of view (0.3 ms) and the long radiative lifetimes for the observed infrared chemiluminescent processes, reactions and quenching (excluding rotational) of the excited species created in the reaction zone can be neglected. Thus, vibrational quenching and $CO(v)$ up pumping [reaction (1b)] can be ignored. The kinetics of $[CO(v,J)]$ are therefore in the steady state and the production rate and the lifetime of the excited species in the field of view

$$d[CO(v,J)]/dt = k[M^*][CO] - \tau_{res}^{-1}[CO(v,J)] = 0, \quad (5)$$

where M^* denotes the excited species created in the microwave discharges responsible for the observed excitation, k is the excitation rate coefficient, and τ_{res} is the residence time in the field of view, 0.3 ms.

Figure 6 shows the absolute vibrational populations for the fit in Fig. 4. The populations for the rotationally excited component exceed those of the 80 K component at all vibrational levels except $v = 1,2$.

As illustrated by Fig. 2 the lowest 80 K CO vibrational populations exhibit a dependence on N_2 mole fraction. We have determined previously[18] that only $N_2(v)$ exhibits a strong variation in its discharge production rate with N_2 mole fraction over the range used here. Thus, relative increases in low CO vibrational population at higher nitrogen mole fraction must be due to the near-resonant energy transfer from $N_2(v)$ [reaction (1a)]. Examination of the populations for all the spectra indicates that only $CO(v = 1,2)$ are affected by nitrogen mole fraction. Since $CO(v)$ up pumping cannot occur under our experimental conditions, the excitation process must be single- and two-quantum transfer

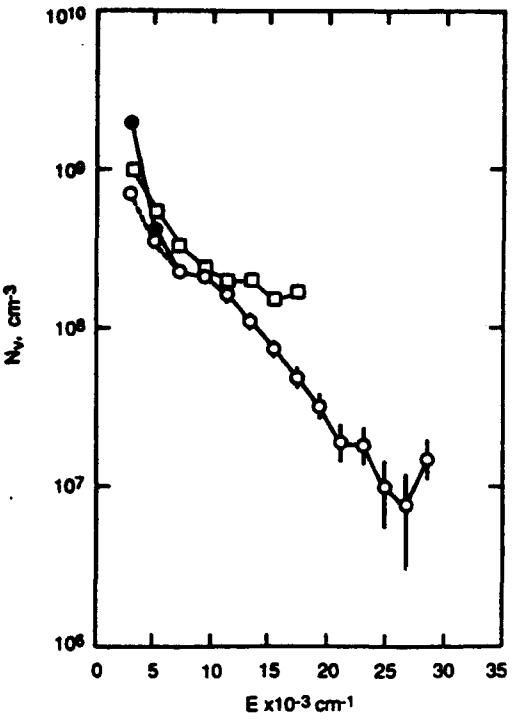

FIG. 6. Determined population distribution vs E_v, for the fit shown in Fig. 4. The thermalized component is shown as (○), with contribution to thermalized $CO(v = 1,2)$ from $N_2(v)$ energy transfer shown as (●), and the rotationally excited component is represented as (□).

$$N_2(v) + CO \rightarrow N_2(v-1) + CO(v=1), \quad (6a)$$

$$N_2(v) + CO \rightarrow N_2(v-2) + CO(v=2). \quad (6b)$$

To determine the relative contribution of the $N_2(v)$ energy transfer process to the $CO(v = 1,2)$ populations, we have plotted the ratios of these populations to $[CO(v = 3)]$ as a function of nitrogen mole fraction. Figure 7 shows one of these plots. Extrapolation of these curves to zero nitrogen mole fraction determines the relative $CO(v = 1,2)$ populations which arise from sources other than energy exchange from $N_2(v = 1,2)$. For the data in Fig. 7, the multiplicative factors are 3.0 and 1.5 for $CO(v = 1,2)$, respectively. The multiplicative factors for all CO mole fractions examined have been determined to be approximately the same.

Using these factors, the contributions to the 80 K $CO(v = 1,2)$ populations from $N_2(v)$ transfer and E–V transfer may be separated. The dotted line in Fig. 6 shows the $CO(v = 1,2)$ number densities corrected for $N_2(v)$ transfer. The vibrational populations of the rotationally excited component exceed those of the 80 K component by typically $\sim 30\%$. This ratio is similar for all the analyzed spectra, showing thereby that neither component exhibits a dependence on nitrogen or carbon monoxide mole fraction.

The $CO(v = 2)$ population attributable to two quantum transfer from $N_2(v)$ is only $6\% \pm 1\%$ of that due to single quantum transfer. This ratio is related to the rate coefficients for reactions (6a) and (6b) in the following manner:

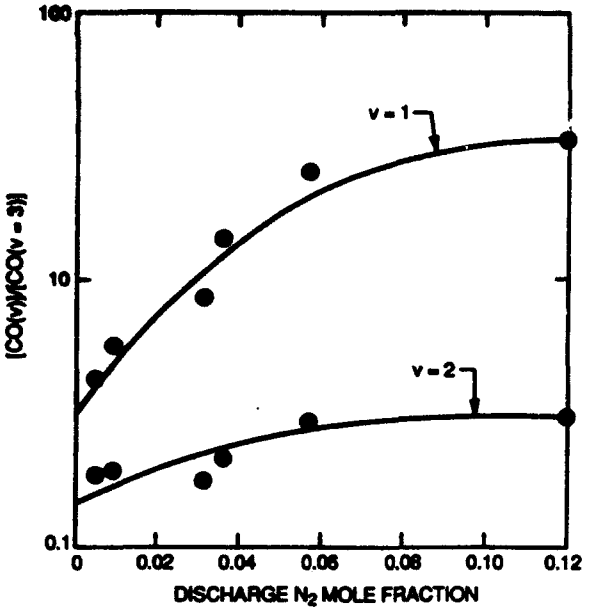

FIG. 7. The plot of the ratio of the $[CO(v=1,2)]$ to $[CO(v=3)]$ populations as a function of nitrogen mole fraction. The CO mole fraction for these data was 0.33.

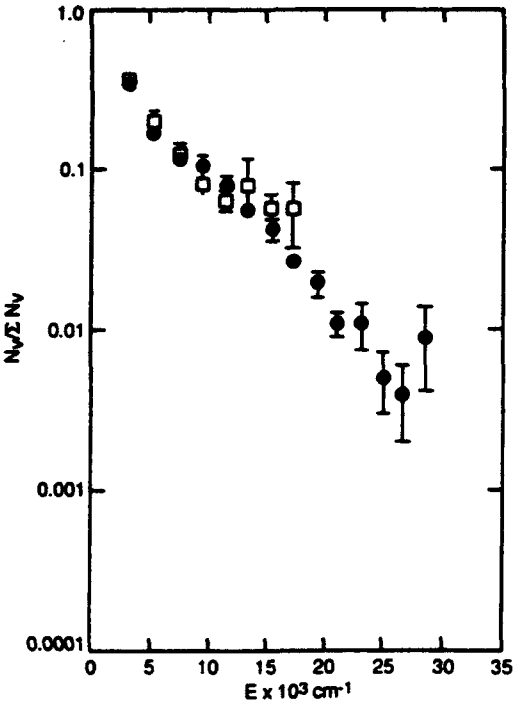

FIG. 8. Averaged relative population distributions for 11 spectra. Both 80 K (●) CO and the rotationally excited components (□) are shown, but have been normalized independently. The error bars represent one standard deviation.

$$\frac{[CO(v=2)]}{[CO(v=1)]} = \frac{\Sigma_v k_v(\Delta v=2)[N_2(v)]}{\Sigma_v k_v(\Delta v=1)[N_2(v)]}. \quad (7)$$

Equation (7) may be resolved if the $N_2(v)$ distribution can be determined. Discharge-flow measurements by Piper and Marinelli using Penning ionization spectroscopy indicate the effluent of microwave discharges employing the conditions encountered here may be represented by a ~6000 K "modified Treanor" distribution in $N_2(v)$.[25] A Treanor distribution contains enhanced populations at higher vibrational levels, relative to a Boltzmann distribution, that are created by collisional up pumping.[14] Using the modified Treanor distribution, we have determined $k_v(\Delta v=2)/k_v(\Delta v=1) = 0.10 \pm 0.04$. Owing to the known increase in k_v as a function of v,[11,12] the ratio determined here is likely representative of higher v (probably 7 to 8). This value falls well within the limits of 0.2 to 0.025 found for all vibrational levels.[26]

Figure 8 shows the average population distributions for the 80 K and rotationally excited components, normalized separately and shown with one standard deviation error bars. The population distributions from 11 spectra were chosen for this average. The spectra containing large contributions to 80 K $CO(v=1,2)$ levels have been excluded since this emission envelope overlaps the $v=5$–8 levels of the rotationally excited component interfering with reliable population determination.

The distributions shown in Fig. 8 are similar, but the distribution of the rotationally excited component appears to be relatively flat above $v=4$. We have examined the data carefully and determined this trend to be accurate. Fits to the data using a fixed relative vibrational distribution of the rotationally excited component following the distribution of the 80 K component seriously underfits the data in the region of $v'=5$–8 of the R-branch bandheads and in the region of the P branches.

EXCITATION MECHANISM

One possible mechanism for rotational excitation of CO is energy transfer from translationally excited atoms emanating from the discharge. Translationally hot H atoms have been reported to excite V,R states of CO.[27] We may discount such processes in our apparatus since we can find no mechanism for hot atom formation and any "hot" atoms that could form in the 1 Torr discharge tubes would be rapidly accommodated. The number density of such species reaching the field of view must therefore be miniscule.

Collisional quenching of high CO vibrational levels into high rotational levels of lower vibrational levels (V,R transfer), analogous to processes observed for HF,[28,29] may also be dismissed. To excite the high J' levels we observed would require nearly gas kinetic multiquantum ($\Delta v \lesssim 8$) quenching of $CO(v)$. This is unlikely since direct measurements of the v-dependent quenching of $CO(v)$ by CO_2 [30] indicate the total quenching rate coefficients to be less than 1% gas kinetic. Under quasiresonance conditions, collisional quenching of diatomics in low v, high J levels into high v, low J levels (R,V transfer) may have rate coefficients of 10^{-11} cm^3 s^{-1}.[31] The resonance conditions are given by

$$\omega_v/\omega_J = \omega_e/4B_eJ. \quad (8)$$

For CO, resonance is satisfied at $J' \sim 120$ which is populated only at the lowest vibrational level for the statistical model. Therefore, R,V transfer should not contribute significantly

to the higher vibrational levels of the observed thermalized emissions.

With other possibilities excluded, the mechanism for $CO(v,J)$ excitation must be energy transfer from one or more of the metastable nitrogen species created in the discharge. We have previously determined that to account for the $CO(v,J)$ excitation observed here, the energy transfer reaction must be at least ~ 3.7 eV exoergic. We use this constraint, combined with kinetic considerations to identify $N_2(a'\,^1\Sigma_u^-)$ as the species responsible for the observed CO excitation.

Summing the populations of the 80 K and rotationally excited components, a product $k[M^*] \sim 0.5\ s^{-1}$ is required to account for the observed emissions. The measured quenching kinetics[32–36] for many of the metastable nitrogen species are shown in Table II. This table contrasts the number densities of the metastable species required in the interaction zone to account for the observed emissions with the number densities determined from modeling studies or direct determination.[18] The number density calculations have employed the room temperature rate coefficients in the absence of data at 80 K.

Quenching reactions of metastable nitrogen atoms are shown in reactions (9) and (10):

$$N(^2D) + CO \rightarrow N(^4S) + CO(v \leq 9), \quad \Delta E = 2.38\ \text{eV}, \quad (9)$$

$$N(^2P) + CO \rightarrow N(^2D) + CO(v \leq 4), \quad \Delta E = 1.196\ \text{eV}, \quad (10a)$$

$$\rightarrow N(^4S) + CO(v \leq 15), \quad \Delta E = 3.576\ \text{eV} \quad (10b)$$

$N(^2D)$ may deposit 2.38 eV into CO rovibrational states, well below the ~ 3.7 eV needed to account for the observed emissions. Additionally, the kinetics of this reaction indicate that contributions to the spectra from this source would be negligible. The energetics of $N(^2P)$ quenching to form $N(^4S)$ matches the required ~ 3.7 eV well. However, the recently determined rate coefficient[32] for quenching of $N(^2P)$ by CO is several orders of magnitude too small for reactions (10a) and (10b) to be the $CO(v,J)$ excitation mechanism.

TABLE II. Measured CO quenching kinetics of N_2^*, N^*.

Species	K_Q (300 K) ($cm^{-3}\,s^{-1}$)	Number density in COCHISE (cm^{-3}): Required for $CO(v,J)$ excitation	Number density in COCHISE (cm^{-3}): Estimated for interaction zone
$N(^2P)$	$<1.5(-14)$[c]	$>3(13)$	1–3(9)
$N(^2D)$	$1.7(-12)$[d]	$>3(11)$	3–10(9)
$N_2(A\,^3\Sigma_u^+)$,			
$v=0$	$1.5(-12)$[b,e]	$>3(11)$	1–3(9)
$v=4$	$1.9(-11)$[b,e]	3(10)	1–3(9)
$N_2(a\,^1\Pi_g)$	$2.8(-10)$[a,f]	2(9)	2(6)
$N_2(a'\,^1\Sigma_u^-)$	$1.1(-10)$[a,g]	4(9)	3(9)

[a] Includes excitation of $CO(A\,^1\Pi)$.
[b] Includes excitation of $CO(a\,^3\Pi)$.
[c] Reference 32.
[d] Reference 33.
[e] Reference 34.
[f] Reference 35.
[g] Reference 36.
Notation: $1(-10) = 1\times10^{-10}$

Excitation of $CO(v<14)$ by energy transfer from $N_2(X,v')$ requires multiquantum transfer from $v'<14$. The contributions to the 80 K $CO(v=1,2)$ populations determined from $N_2(v)$ energy transfer are consistent with a preferred channel for single-quantum exchange and a less favored channel for two-quantum exchange. Therefore, we do not believe multiquantum exchange from $N_2(X,v')$ can be the responsible excitation mechanism.

$N_2(A\,^3\Sigma_u^-)$ quenches with CO to form $CO(a\,^3\Pi)$.[34] Although the

$$N_2(A\,^3\Sigma_u^-) + CO \rightarrow N_2(X) + CO(a\,^3\Pi), \quad (11)$$

$$CO(a\,^3\Pi) + CO \rightarrow 2CO(X, 5 \leq v \leq 13) \quad (12)$$

rate coefficient for the quenching process is known,[34] the absolute yield for reaction (11) has not been measured. Reaction of $CO(a)$ with another CO molecule produces vibrationally excited CO[37,38] with a nearly gas-kinetic rate coefficient for the process ($k_{12} \sim 1\times10^{-10}\ cm^3\,s^{-1}$ at room temperature).[39,40] Quenching of $N_2(A)$ may produce rovibrationally excited CO directly from a branch in reaction (11). Since $N_2(A)$ lies 6.17 eV above $N_2(X,v=0)$, such a process would be sufficiently energetic. The $N_2(A)$ quenching rate coefficient, however, is too small for this process or any derived reactions, such as reaction (12), to be responsible. Additionally, the activation barrier determined for this process by Slanger *et al.*[41] indicates the rate constant may be smaller, $<10^{-13}\ cm^3\,s^{-1}$, at 80 K.

The $N_2(W\,^3\Delta_u, w\,^1\Delta_u)$ states lie 7.36 and 7.35 eV above the ground state, respectively, and are sufficiently energetic to produce the observed $CO(v,J)$ emissions. The quenching reactions of these two species have not been reported in the literature, however. We have determined $N_2(W\,^3\Delta_u, v=1\text{–}5)$ and $N_2(w\,^1\Delta_u, v=0\text{–}2)$ number densities in COCHISE directly from their IR radiance over the 2–4 μm region.[22] Their concentrations in the interaction region are typically 3×10^8 and 1×10^8 molecules cm^{-3}, respectively. Even if these species quench CO with rate coefficients near gas kinetic, they cannot account for the observed $CO(v,J)$ emissions.

Quenching of $N_2(a\,^1\Pi)$ is rapid, forming $CO(A\,^1\Pi)$.[15,35] Although the

$$N_2(a\,^1\Pi) + CO \rightarrow N_2(X,v) + CO(A\,^1\Pi) \quad (13)$$

yield of $CO(A)$ formation from this reaction is large,[15] a channel forming $CO(v,J)$ is possible. $N_2(a)$ may deposit any fraction of the available 8.4 eV into CO rovibrational states from such a process. However, the radiative lifetime of $N_2(a)$ is short, $56 \pm 4\ \mu s$,[42] which makes the number density of this species in the interaction zone to be too small to account for the observed emissions. The upper limit for $N_2(a)$ number density shown in Table II has been determined from the noise level of discharged Ar/N_2 spectra at the wavelength $N_2(a-a')$ features would occur,[22] and is consistent with the expected radiative decay of $N_2(a)$ in the 0.5 ms collisionless expansion between the discharge exit and the reaction zone.

The possible quenching reactions of the $N_2(a'\,^1\Sigma_u^-)$ with CO are

$$N_2(a'\,^1\Sigma_u^-) + CO \rightarrow N_2(X,v) + CO(A\,^1\Pi), \quad (14a)$$

$$\rightarrow N_2(X,v) + CO(X,v,J), \quad (14b)$$

$$\rightarrow N_2(X,v) + CO(I\,^1\Sigma^-, D\,^1\Delta). \quad (14c)$$

$N_2(a')$ may deposit up to 8.5 eV into CO electronic, vibrational, and rotational states. The branching ratio forming $CO(A)$ has been measured as $20^{+10}_{-8}\%$.[36] This value, however, was based on an 80^{+40}_{-20} μs lifetime for the $N_2(a)$ state which has recently been revised to be 56 ± 4 μs.[42] The corrected $CO(A)$ branching ratio is $30\% \pm 8\%$. The remaining fraction must be divided between the other energetically accessible spin-allowed channels. These channels are rovibrationally excited $CO(X)$ [reaction (14b)] and $I\,^1\Sigma^-$ and $D\,^1\Delta$ states [reaction (14c)]. At room temperature, the total quenching rate constant for reaction (14) is 1.1×10^{-10} $cm^3\,s^{-1}$.[36] Table II shows that the kinetics of this reaction are sufficient to account for the observed emissions.

Since $N_2(a')$ is the only species present in the interaction zone that satisfies both the kinetic and energetic constraints, we postulate that reaction (14b) must be responsible for the observed $CO(v,J)$ excitation. For this hypothesis to be correct, the branching fraction for reaction (14b) must be relatively large, constraining reaction (14c) to be small and, owing to the short radiative lifetime of $CO(A)$, the 80 K populations must reflect a contribution from $CO(A)$ radiative cascade.

DISCUSSION

In the preceding discussion, we identified $N_2(a'\,^1\Sigma_u^-)$ to be the species responsible for the observed $CO(v,J)$ excitation. We show in this section that simple models incorporating reactions (14a) and (14b) can account for the observed vibrational distributions for both the 80 K and rotationally excited components. Surprisal analysis of the rotationally excited component vibrational distribution indicates two mechanisms are responsible and vibrational levels greater than eight are predicted. We then demonstrate that the 80 K vibrational distributions can be modeled by contributions from $CO(A)$ radiative cascade and the rotationally excited component. The latter may arise either from rotational relaxation or initial bimodality in the energy transfer reaction.

Surprisal theory[43,44] postulates the existence of an exponential gap law for an individual metathetic reaction

$$P_v = P^0(v)\exp(-\lambda f_v)/\exp(\lambda_0), \quad (15)$$

where f_v is the fraction of the reaction exoergicity appearing as vibrational energy in the product, $P(v)$ is the observed relative vibrational population, and $P^0(v)$ is the statistical "prior" distribution obtained when all final translational, rotational, and vibrational states are equally probable. Thus, the ratios of the observed and statistical vibrational populations should be exponential in the vibrational energy E_v, with the exponential fall-off constant λ quantifying the departure of the observed distribution from a completely statistical product distribution. While this theory does not necessarily hold for all chemical interactions, it has proved useful in the analysis of rovibrational product distributions from several photochemical and reactive interactions.

Both the vibrational extent of the 80 K CO emission ($v \leq 14$, $E \sim 3.4$ eV) and the rovibrational excitation of the rotationally excited component ($E_T \sim 3.7$ eV) can be attributed to an energy transfer process of 3.5–3.7 eV. Using a prior distribution for 3.7 eV determined from the usual relationship for a vibrating rotator,[43,44]

$$P^0(v) = (1 - f_v)^{3/2} \sum_{v=0}^{v^*} (1 - f_v)^{3/2} \quad (16)$$

the vibrational surprisal plot for the vibrational populations of the rotationally excited component has been plotted in Fig. 9. The change in slope indicates two dynamic mechanisms are responsible for the rotationally excited component: one accounting principally for $v = 1$–4 and another for the higher vibrational levels. The relative populations of the rotationally excited component may be reproduced by a model composed of two such mechanisms as shown in Fig. 10. The model is comprised by roughly equal contributions from a low v excitation process and a "statistical" process which contributes to all vibrational levels. The distribution used for the statistical process is the prior calculated for 3.7 eV. This model predicts populations for $v > 8$ of the rotationally excited component. Absolute populations of these levels cannot be determined from the spectra due to the overlap of these bands with the 80 K CO emission features. However, we have performed fits to the data using $v = 1$–14 of the rotationally excited component following the modeled distribution shown in Fig. 10. The resulting fits do not exhibit any marked differences from fits excluding $v > 8$ of the rotationally excited component and the match to the absolute intensity in the P-branch region is generally improved. Under these conditions, the populations determined for $v > 4$ of the 80 K component are decreased by an average of ~40%.

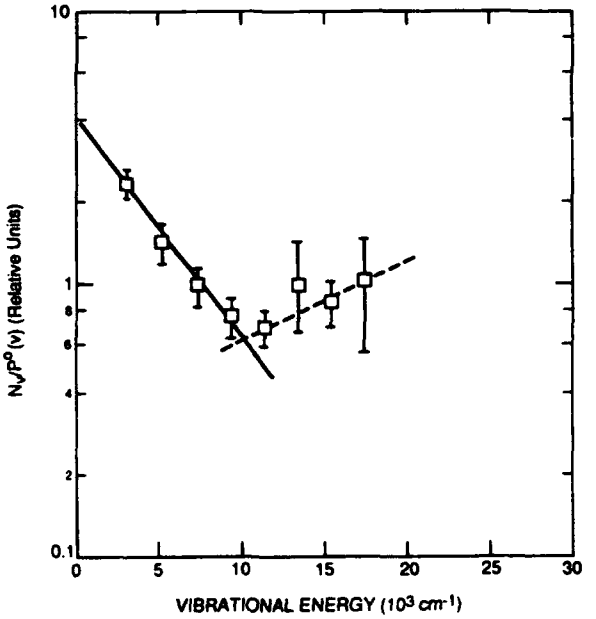

FIG. 9. Vibrational surprisal plot for the rotationally excited vibrational populations. The populations are those from Fig. 8.

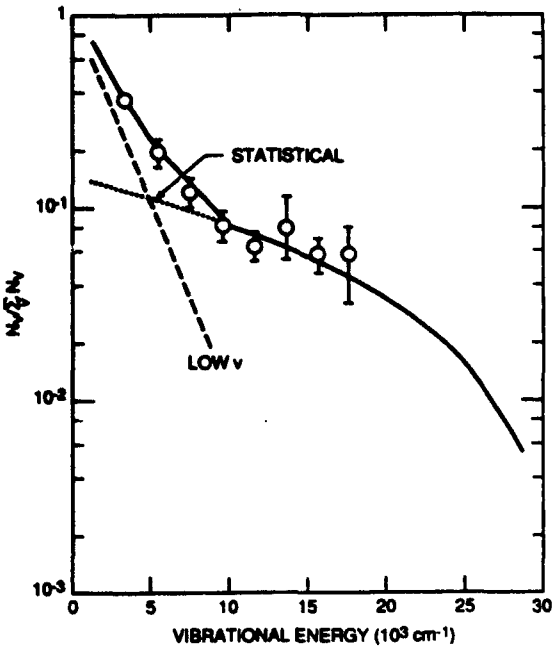

FIG. 10. Model fit to the rotationally excited vibrational populations. The model, shown by a solid line, has been produced by equal contributions from the low v ($v \leq 4$) (---) mechanism and the statistical mechanism (all v) (···).

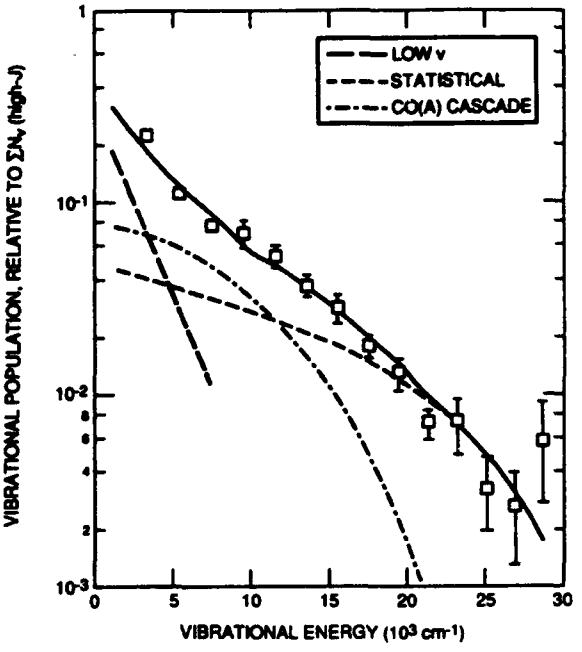

FIG. 11. Model fit to the 80 K vibrational populations. The model (—) has been produced by a contribution of 14% branching fraction from reaction (14a), (- - -) and 30% of the rotationally excited model, shown separately as low v (– –) and statistical contributors (---). The relative populations have been normalized to the sum of the rotationally excited vibrational populations.

Thus, the populations for $v > 8$ of the 80 K component shown in Fig. 8 represent upper limits.

Due to the implications of the model and the improvement in the P-branch fits, we believe that $v > 8$ of the rotationally excited component are present in the data. However, higher resolution studies will be required to confirm their presence and determine the true population distribution.

The 80 K component must include contribution from reaction (14a) to the vibrational populations due to CO(A) radiative cascade. Quenching of $N_2(a'\,{}^1\Sigma_u^-, v = 0)$ via reaction (14a) yields CO($A\,{}^1\Pi, v \leq 2$).[36] Owing to the short radiative lifetime of the CO(A) state, ~10 ns, all of the CO(A) created by this process under our experimental conditions will cascade radiatively to form CO($v \leq 9$) with a vibrational distribution reflecting the known branching ratios. The rotational temperature of the CO(A) states formed in this manner have been determined to be approximately 1000 K.[36] This amount of rotational excitation is modest and the resulting CO(X) states formed by radiative cascade will be rapidly thermalized within the residence time in the field of view (20–30 collisions).

It is reasonable to expect that relaxation of the rotationally excited component may also contribute to the observed 80 K component populations. Using only CO(A) radiative cascade and rotational relaxation of the rotationally excited component, we have successfully modeled the 80 K vibrational distribution as shown in Fig. 11. The contribution to the model from the rotationally excited component is shown in Fig. 11 as the low v and statistical distributions from Fig. 10. Reproduction of the absolute distribution requires roughly 30% of the rotationally excited component to be thermalized (relaxed) and a branching fraction for CO(A) excitation of 14%. The determined contribution from CO(A) radiative cascade is about a factor of 2 lower than the recalculated branching ratio of Piper.[36] Our result could be consistent, however, if the branching ratio for reaction (14a) decreases somewhat at lower temperatures. As an alternative to rotational relaxation of the rotationally excited component, the initial distribution may be bimodal. We cannot distinguish, however, between these scenarios under our experimental conditions.

In summary, the results of surprisal analysis indicate two dynamic mechanisms are responsible for the rotationally excited component, one producing the low vibrational levels and the other, a statistical mechanism that contributes to all vibrational levels. CO(A) radiative cascade and relaxation of a fixed fraction of the rotationally excited component are sufficient to account for the 80 K populations.

The dynamics of the $N_2(a')$ + CO quenching process are worthy of some comment. The interaction must satisfy conservation of angular momentum and energy

$$(2\mu E_i)^{1/2} b_i = (2\mu E_f)^{1/2} b_f + Jh/2\pi, \tag{17}$$

$$E_i + \Delta E = E_f + E_r + BJ^2, \tag{18}$$

where μ is the reduced mass, E_i and E_f are the initial and final center-of-mass collision energies, b_i and b_f are the initial and final impact parameters, ΔE is the exoergicity of the process, and BJ^2 approximates the product rotational energy after the collision. From Eq. (17), large values of J can be

achieved through highly attractive collisions with large initial impact parameters and small final impact parameters with the concurrent requirement that the final center-of-mass kinetic energy is small.[45] This then suggests a long-range attraction between $N_2(a')$ and CO, similar to that inferred for $N_2(a) + CO$.[15] The implication from surprisal analysis, that there are at least two dynamic mechanisms for reaction (14b), further suggests a strong anisotropy in the potential energy surface, by analogy to observations of $CO(v,J)$ formed in the quenching of $Na(3\,^2P)$ by CO.[8] Clearly, detailed potential energy surface calculations are required to test this hypothesis.

CONCLUSIONS

We have observed extensive rovibrational excitation in carbon monoxide from quenching of discharged nitrogen in a low pressure cryogenic apparatus. Analysis of the data has identified a contribution to $CO(v = 1,2)$ of the 80 K component from

$$N_2(v) + CO \rightarrow N_2(v-1) + CO(v=1)$$
$$N_2(v) + CO \rightarrow N_2(v-2) + CO(v=2).$$

Based on kinetic and energetic arguments, we have determined the energy transfer process

$$N_2(a'\,^1\Sigma_u^-) + CO \rightarrow N_2(X,v) + CO(A\,^1\Pi)$$
$$\rightarrow N_2(X,v) + CO(v,J)$$

to be responsible for the observed rovibrational excitation.

The energy transfer collisions producing the rotationally excited component exhibit complex dynamic behavior, two dynamic mechanisms have been identified, one responsible for low vibrational levels and another that contributes to all accessible vibrational levels. Rigorous potential energy surface calculations will be required, however, to determine the true dynamics of the $N_2(a') + CO$ interaction.

ACKNOWLEDGMENTS

The authors would like to acknowledge advice provided by B. D. Green, W. A. M. Blumberg, K. W. Holtzclaw, L. G. Piper, and W. J. Marinelli, and assistance provided by H. C. Murphy, M. Gouveia, and M. DeFaccio. This work was performed under Contract No. F19628-85-C-0032 with the Air Force Geophysics Laboratory and was sponsored by the U.S. Air Force Office of Scientific Research under Task No. 2310G4 and by the Defense Nuclear Agency under Project SA, Task SA, Work Unit 115.

[1]P. L. Houston, J. Phys. Chem. 91, 5388 (1987).
[2]E. L. Woodbridge, T. R. Fletcher, and S. R. Leone, J. Phys. Chem. 92, 5387 (1988).
[3]D. J. Bamford, S. V. Filsith, M. F. Foltz, J. W. Hepburn, and C. B. Moore, J. Chem. Phys. 82, 3032 (1985).
[4]D. Debarre, M. Lefebvre, M. Pealat, J. P. E. Taran, D. J. Bamford, and C. B. Moore, J. Chem. Phys. 83, 4476 (1985).
[5]D. R. Harding, R. E. Weston, and G. W. Flynn, J. Phys. Chem. (in press).
[6]R. G. Shortridge and M. C. Lin, J. Chem. Phys. 64, 4076 (1976).
[7]D. S. Y. Hsu and M. C. Lin, Chem. Phys. Lett. 42, 78 (1976).
[8]W. Reiland, H. U. Tittes, I. V. Hertel, V. Bonacic-Koutecky, and M. Persico, J. Chem. Phys. 77, 1908 (1982).
[9]M. C. Lin and R. G. Shortridge, Chem. Phys. Lett. 29, 42 (1974).
[10]H. Horiguchi and S. Tsuchiya, J. Chem. Phys. 70, 762 (1979).
[11]S. DeBenedictis and F. Cramarossa, Chem. Phys. 112, 363 (1987).
[12]S. DeBenedictis, M. Capitelli, F. Cramarossa, R. D'Agostino, and C. Gorse, Chem. Phys. Lett. 112, 54 (1984).
[13]C. E. Treanor, J. W. Rich, and R. G. Rehm, J. Chem. Phys. 48, 1978 (1967).
[14]G. E. Caledonia and R. E. Center, J. Chem. Phys. 55, 552 (1971).
[15]G. Sha, D. Proch, and L. Kompa, J. Chem Phys. 7, 2742 (1987).
[16]J. W. Dreyer, D. Perner, and C. R. Roy, J. Chem. Phys. 61, 3164 (1974).
[17]W. T. Rawlins, H. C. Murphy, G. E. Caledonia, J. P. Kennealy, F. X. Robert, A. Corman, and R. A. Armstrong, Appl. Opt. 23, 3316 (1984).
[18]W. T. Rawlins, M. E. Fraser, and S. M. Miller, J. Phys. Chem. 93, 1097 (1989).
[19]N. Legray-Sommaire and F. Legay, Can. J. Phys. 48, 1966 (1970).
[20]N. Washida, H. Bandow, and G. Ionoue, Bull. Chem. Soc. Jpn. 56, 3748 (1983).
[21]R. Farrenq, C. Rossetti, G. Guelachvili, and W. Urban, Chem. Phys. 92, 389 (1985).
[22]M. E. Fraser, W. T. Rawlins, and S. M. Miller, J. Chem. Phys. 88, 538 (1988).
[23]K. P. Huber and G. Herzberg, *Molecular Spectra and Molecular Structure. IV. Constants of Diatomic Molecules* (Van Nostrand Reinhold, New York, 1979).
[24]C. Chackerian, R. Farrenq, G. Guelachvili, C. Rossetti, and W. Urban, Can. J. Phys. 62, 1579 (1984).
[25]L. G. Piper and W. J. Marinelli, J. Chem. Phys. 89, 2918 (1988).
[26]G. D. Billing (private communication).
[27]G. K. Chawla, G. C. McBane, P. L. Houston, and G. C. Schatz, J. Chem. Phys. 8, 5481 (1988).
[28]H. K. Haugen, W. H. Pence, and S. R. Leone, J. Chem. Phys. 80, 1839 (1984).
[29]X. F. Yang and G. C. Pimentel, J. Chem. Phys. 81, 1746 (1984).
[30]G. E. Caledonia, B. D. Green, and R. E. Murphy, J. Chem. Phys. 71, 4369 (1979).
[31]B. Stewart, P. D. Magill, T. P. Scott, J. Derouard, and D. E. Pritchard, Phys. Rev. Lett. 60, 282 (1988).
[32]W. T. Rawlins, L. G. Piper, M. E. Fraser, and H. C. Murphy, PSI 9032/TR-901, Final Report, Contract F19628-85-C-0032, February 1989.
[33]L. G. Piper, M. E. Donahue, and W. T. Rawlins, J. Chem. Phys. 91, 3883 (1987).
[34]J. M. Thomas, F. Kaufman, and M. F. Golde, J. Chem. Phys. 86, 6885 (1987).
[35]W. J. Marinelli, W. J. Kessler, B. D. Green, and W. A. M. Blumberg, J. Chem. Phys. 90, 2167 (1989).
[36]L. G. Piper, J. Chem. Phys. 7, 1625 (1987).
[37]T. G. Slanger, G. Black, and J. Fournier, J. Photochem. 4, 329 (1975).
[38]Yu.Z. Ionikh, A. L. Kuranov, A. A. Lobanov, and L. S. Starenkova, Opt. Spectrosc. (USSR) 60, 444 (1986).
[39]G. W. Taylor and D. W. Setser, J. Chem. Phys. 58, 4840 (1973).
[40]W. G. Clark and D. W. Setser, Chem. Phys. Lett. 33, 71 (1975).
[41]T. G. Slanger, B. J. Wood, and G. Black, J. Photochem. 2, 63 (1973).
[42]W. J. Marinelli, W. J. Kessler, B. D. Green, and W. A. M. Blumberg, J. Chem. Phys. 91, 701 (1989).
[43]R. B. Bernstein and R. D. Levine, in *Advances in Atomic and Molecular Physics II*, edited by D. R. Bates and B. Bederson (Academic, New York, 1975), p. 216.
[44]R. D. Levine and R. B. Bernstein, in *Modern Theoretical Chemistry, Vol. III: Dynamics of Molecular Collisions Part B*, edited by W. H. Miller (Plenum, New York, 1975), Chap. 7.
[45]D. Poppe, Chem. Phys. 111, 17 (1987); 111, 21 (1987).

Reprinted from

THE JOURNAL

OF

CHEMICAL PHYSICS

VOLUME 96 NUMBER 10

15 MAY 1992

Branching ratios for infrared vibrational emission from NO($X^2\Pi$,v' =2–13)

W. T. RAWLINS and M. E. FRASER
Physical Sciences Inc., 20 New England Business Center, Andover, Massachusetts 01810

STEVEN M. MILLER and W. A. M. BLUMBERG
Phillips Laboratory/Geophysics Directorate, Hanscom Air Force Base, Massachusetts 01731

pp. 7555-7563

Published by the

AMERICAN INSTITUTE OF PHYSICS

AIP

Branching ratios for infrared vibrational emission from NO($X\,^2\Pi, v' = 2$–13)

W. T. Rawlins and M. E. Fraser
Physical Sciences Incorporated, 20 New England Business Center, Andover, Massachusetts 01810

S. M. Miller and W. A. M. Blumberg
Phillips Laboratory/Geophysics Directorate, Hanscom Air Force Base, Massachusetts 01731

(Received 14 November 1991; accepted 30 January 1992)

The ratios of overtone and fundamental vibrational Einstein coefficients for NO($X\,^2\Pi$) have been measured by spectrally resolved infrared chemiluminescence near 2.7–3.3 μm and 5.2–6.8 μm. The reactions of N(^2D,^2P) with O_2, in the presence of a small background of He in a cryogenic low-pressure reactor, generated vibrationally excited, rotationally cold (60 K) NO(v), whose emission spectra were recorded with high spectral resolution. Least-squares spectral fitting analysis of the observed overtone and fundamental spectra gave vibrational band intensities, whose ratios at each emitting vibrational level v' yielded the $(\Delta v = 2)/(\Delta v = 1)$ Einstein coefficient ratios for $v' = 2$–13. The results provide comparisons to previous theoretical and experimental data, and reflect the behavior of the dipole moment function for NO($X\,^2\Pi$). The measured ratios indicate an overtone Einstein coefficient $A_{2,0} = 0.94 \pm 0.11\ s^{-1}$ for an assumed fundamental value $A_{1,0} = 13.4\ s^{-1}$.

I. INTRODUCTION

The nitric oxide molecule plays key roles in the chemistry and radiative behavior of air-breathing combustion systems, chemical lasers, discharge plasmas, and the earth's atmosphere. In all of these applications, the infrared vibrational transition probabilities for NO are important for diagnostic applications and investigations of energy/radiation transfer. Owing to the high temperatures and nonequilibrium conditions in which NO radiation is often encountered, the emitting species can be highly internally excited, requiring knowledge of vibration–rotation transition moments at large internuclear separations. This information for NO is available only from theory, with little or no experimental validation. In this paper, we present experimental data for the branching ratios of fundamental and first overtone emission from highly vibrationally excited NO, as observed in a cryogenic chemiluminescence reactor. These data provide insight into the shape of the electric dipole moment function, as well as an indirect determination of the absolute $(v' = 2) \rightarrow (v'' = 0)$ overtone transition probability.

In the specification of absolute emission intensities and spectral distributions, one requires the vibrational emission rates (Einstein coefficients, $A_{v',v''}$), averaged over all thermally populated rotational levels, for all the vibrational states of interest. While many ground state absorption measurements have determined values for the $(v',v'') = (1,0)$ and (2,0) transition strengths, the scaling of $A_{v',v''}$ with v' is only partially understood. Previous empirical determinations[1,2] of the dipole moment near equilibrium internuclear separation provided limited information for low v'. In a definitive theoretical treatment, Billingsley[3–6] performed an *ab initio*, multiconfiguration self-consistent-field (MCSCF) calculation of the dipole moment function of NO($X\,^2\Pi$), and rigorously evaluated the rotationally dependent and thermally averaged Einstein coefficients for the fundamental ($\Delta v = 1$) and first overtone ($\Delta v = 2$) transitions over a large range of v' and J' ($v' = 1$–20, $J' = 0.5$–33.5). The overlap of the *ab initio* dipole moment function and the NO($X\,^2\Pi$) potential is illustrated in Fig. 1. The absolute values and relative scalings given by this work have been widely utilized; however the absolute values of $A_{v',v''}$ are now known to be erroneously small.[7]

In the only previous experimental investigation of vibrational dependence, Green *et al.*[8] determined Einstein coefficient branching ratios for NO($v' = 2$–9) from $\Delta v = 1$ and $\Delta v = 2$ fluorescence spectra in electron-bombarded N_2/O_2 mixtures. These measurements confirmed Billingsley's[6] predicted vibrational scaling of the branching ratios for $v' = 3$–7, and established that the dipole moment function of Michels[1] was incorrect. However, the experimental data leave considerable uncertainty for the (2,0)/(2,1) ratio, and are not definitive for $v' > 8$. Nevertheless, the data of Green *et al.*[8] verify the shape (second derivative) of the *ab initio* dipole moment function at intermediate nuclear separation. Thus, a reasonable approach for selecting values of $A_{v',v''}$ is to apply the Billingsley[6] vibrational scalings to absolute values of $A_{1,0}$ and/or $A_{2,0}$ determined from careful absorption measurements.[2,9,10] This approach was adopted by Rothman *et al.*[7] to evaluate absorption strengths for both the fundamental and the first overtone; the resulting absolute values were slightly modified by Rawlins *et al.*[11] for the analysis of NO($\Delta v = 1$) chemiluminescence spectra.

We have previously reported[11] detailed laboratory investigations of the vibrational chemiluminescence from nascent NO(v,J) formed by reactions of metastable atomic nitrogen with O_2, as originally observed by Kennealy *et al.*[12] In the recent experiments,[11] extensive rotational and vibrational excitation was observed in nitric oxide formed under nearly collisionless conditions by the reactions

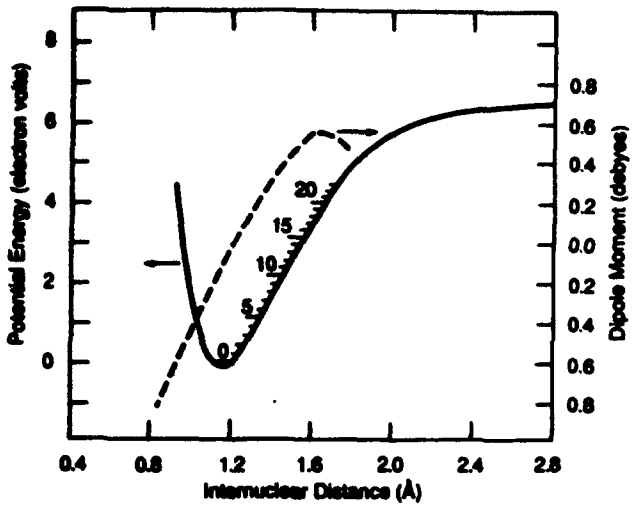

FIG. 1. *Ab initio* dipole moment function of Billingsley (Refs. 3 and 4) compared to potential curve for NO($X\,^2\Pi$).

$$N(^2D) + O_2 \rightarrow NO(v) + O(^1D,^3P), \quad \text{(R1)}$$

$$N(^2P) + O_2 \rightarrow NO(v,J) + O(^1S,^1D,^3P). \quad \text{(R2)}$$

The NO(v) distributions from (R1) peak near $v = 7$, and are detectable to $v = 14$. Reaction (R1) is responsible for auroral chemiexcitation of NO(v),[13,14] and for most of the production of NO in the earth's thermosphere.[15]

Reaction (R2) produces NO(v,J) with a high degree of rotational excitation in each of several (at least eight) vibrational levels.[11] The spectral data exhibit distinctive *R*-branch band heads, which signify substantial populations of rotational states in the range $J = 60.5$–120.5 (i.e., > 1 eV of rotational energy). Similar band heads have been observed in high-altitude auroral spectra of NO emission,[16] indicating a significant role for (R2) and/or similar chemiexcitation processes in the particle-bombarded upper atmosphere.

In the analysis of spectral distributions for the high vibrational and rotational states populated by reactions (R1) and (R2), it is necessary to probe the dipole moment function over a much larger range of the NO potential surface than has previously been examined experimentally. In addition, it is often important to specify the overtone spectral distribution corresponding to that of the fundamental, or vice versa. To these ends, we have used the infrared chemiluminescence approach, previously applied to determine the nascent product distributions for reactions (R1) and (R2), to simultaneously observe $\Delta v = 1$ and $\Delta v = 2$ spectral distributions from those reactions. To eliminate complications due to multimodal rotational distributions and spectral band overlap, we introduced low levels of helium bath gas which caused extensive rotational cooling and slight vibrational deactivation of the initial state distributions. This effect, combined with the cryogenic temperature of the reaction chamber, resulted in extremely low-temperature Boltzmann rotational distributions, which permitted accurate determinations of the $(\Delta v = 2)/(\Delta v = 1)$ branching ratios over the range $v' = 2$–12. The results clarify previous determinations at low v', and indicate significant departure from Billingsley's[6] scaling at high v'.

A subsequent paper[17] will address the analysis of the branching ratios to determine an empirical dipole moment function for NO and the corresponding Einstein coefficients. We describe here the experimental methods, spectral analysis, and branching ratio results as compared with previous work.

II. EXPERIMENTAL MEASUREMENTS

The experiments were performed in the cryogenic COCHISE (cold chemiluminescent infrared stimulation experiment) facility at the Geophysics Directorate. The design and operation of this facility are described in detail elsewhere;[18] the measurement conditions were essentially the same as those for the previous NO chemiluminescence investigation.[11] In brief, the reaction cell and surrounding radiative environment are cooled to approximately 15–20 K, which eliminates background radiation and provides rapid cryopumping of the reagent gases. The infrared detection system consists of a cryogenic, scanning grating monochromator and a liquid-helium–cooled Si:As detector, focused to infinity along the axis of the reaction cell. Reagent gases, at 80 K, enter the cell through a series of four opposing jets, and mix along the cell axis as illustrated in Fig. 2. In the present case, nitrogen metastables, generated by microwave discharge of flowing N_2/Ar (12% N_2) mixtures near 1 Torr, enter from one side of the cell and mix along the centerline with a mass-balanced opposing flow of O_2. This results in a rapid chemical reaction producing chemiexcited NO(v,J), which radiates in infrared bands near 5.4 ($\Delta v = 1$) and 2.7 ($\Delta v = 2$) μm. The discharges are modulated with a 23 Hz square wave, and the emission from the reaction zone is observed via phase-sensitive detection.

In other applications of this technique,[19–21] the pressure in the reaction zone is typically 3–5 mTorr, approaching single collision conditions. For the present experiments, he-

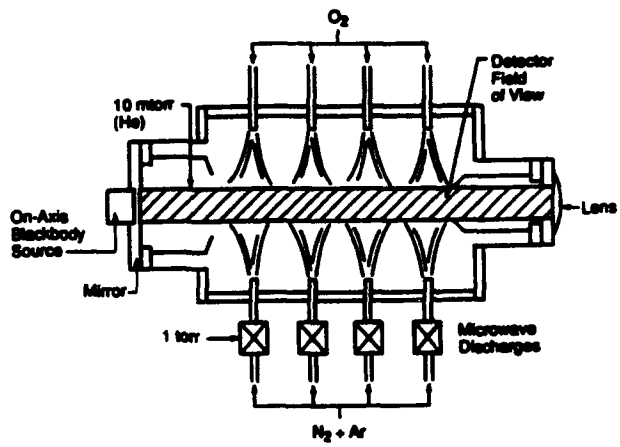

FIG. 2. Diagram of COCHISE reaction chamber.

lium was admitted to achieve a steady state (static) pressure of 10 mTorr, quenching out the high-J states. Preliminary measurements in the absence of He gave overtone spectra which were difficult to analyze unambiguously, owing to the extensive spectral overlap between poorly resolved high-J and thermalized rotational components of adjacent vibrational bands. The addition of small amounts of He resulted in significant rotational cooling, and a pressure of 10 mTorr was sufficient to eliminate the high-J components. This is demonstrated by the absence of R-branch band heads in the $\Delta v = 1$ spectra, and by the conformity of the rotational distributions to a single-temperature Boltzmann form for all vibrational levels.

Spectra of the $\Delta v = 1$ and $\Delta v = 2$ emission were recorded sequentially, as matched pairs, using order-sorting interference filters to isolate each band. A total of four matched pairs were recorded, all for essentially the same conditions of pressure, temperature, flow rates, and discharge operation. All spectra were obtained at a resolution of 0.0067 μm (full width at half-maximum), corresponding to approximately 2.3 cm^{-1} for the fundamental band and 9.2 cm^{-1} for the overtone band. The uncertainty in the observed wavelengths is $\pm$ 0.003 μm due to a periodic fluctuation in the monochromator scan rate at cryogenic temperature.

Before and after the spectral measurements, the optical system was calibrated for absolute and relative spectral response using a blackbody radiation source imbedded in the mirror at the end of the reaction cell. The calibrations employed blackbody temperatures between 350 and 400 K, with a temperature measurement uncertainty of $\pm$ 3 K. This results in a systematic uncertainty of $\pm$ 12% in the measured $(\Delta v = 2)/(\Delta v = 1)$ intensity ratios.

A representative spectral pair is shown in Fig. 3, with the NO transition band centers labeled. Note the logarithmic intensity scale illustrating a dynamic range of approximately two orders of magnitude. The NO($\Delta v = 1$) system is clearly resolved up to $v' = 13$, with no apparent interfering radiators. However, several additional features appear with the NO($\Delta v = 2$) system. The (5,2) and (2,0) bands of the N_2 ($W^3\Delta_u \rightarrow B^3\Pi_g$) electronic transition[22] are evident near 2.6 and 3.3 μm, respectively; the 3.3 μm band ultimately limits the range of v' for which the analysis can be carried out. In addition, several Rydberg transitions of Ar are observable as scattered light from the discharges.[23] In particular, a weak Ar line near 2.69 μm partially obscures the NO($2 \rightarrow 0$) emission, necessitating a factor of $\approx$2 downward correction in the observed intensity of this band.

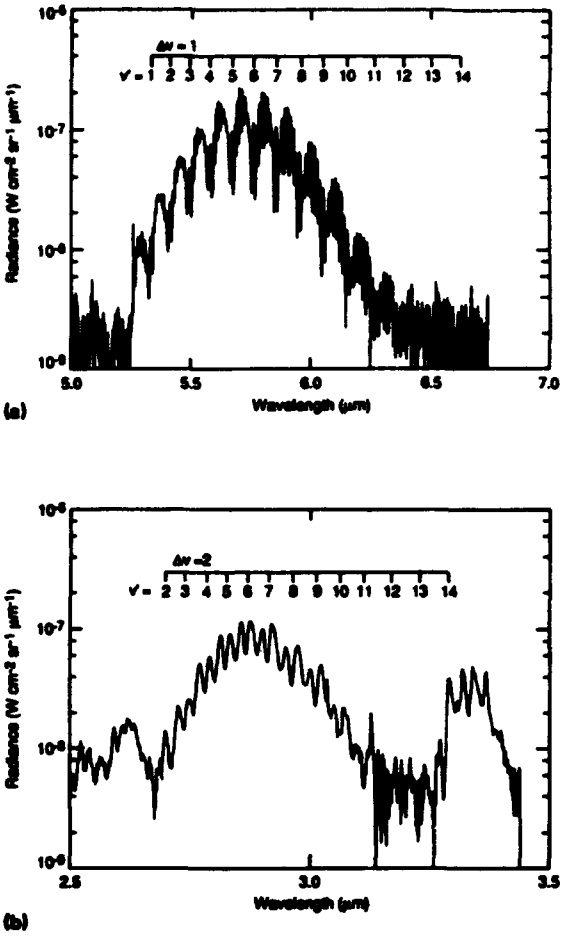

FIG. 3. Observed fundamental and overtone emission spectra. Band centers of the individual vibrational transitions are indicated.

III. ANALYSIS AND RESULTS

The spectra were analyzed using a linear least-squares spectral fitting method which we have employed extensively in the past.[11,12,15,18-21] The NO line positions and strengths were calculated with the spectroscopic constants given in Rawlins *et al.*[11] (as modified slightly from those of Goldman and Schmidt[24]) using the assumption of Hönl–London scaling of the rotational line strengths.[25] From the predictions of Billingsley,[5,6] the Hönl–London assumption should be accurate for the low-J levels sampled in these measurements. In particular, spin-uncoupling and vibration–rotation interactions will not impact the analysis of the data. Matching of the observed rotational envelopes to the computed spectra gives a uniform rotational temperature of 60 K, signifying that the presence of He causes significant thermal coupling between the 80 K reagent gases and the 20 K reactor wall. At 60 K, the third rotational level carries the maximum population, and 99% of the population lies in the lowest ten rotational levels. Examples of the computed spectral fits are shown in Figs. 4 and 5.

The least-squares solutions to the spectral fitting procedure are the integrated intensities for each vibrational transition, $[NO(v')]A_{v',v''}$, as plotted in Fig. 6 for a matched pair of overtone and fundamental spectra. By taking ratios of these values at each v' for a given spectral pair, we determine the Einstein coefficient ratios $A_{v',v''-2}/A_{v',v''-1}$, which represent the branching ratios between $\Delta v = 2$ and $\Delta v = 1$ transitions. The observed Einstein coefficients are thermally

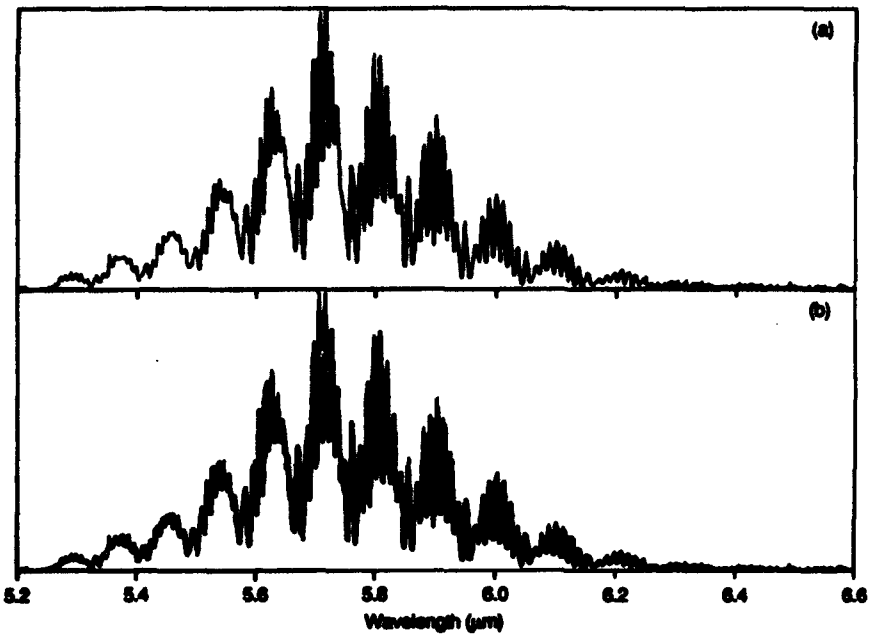

FIG. 4. Data (light line, shown with best fit and separately above) and least-squares fit (dark line) to NO($\Delta v = 1$) emission spectrum. Rotational temperature and spectral resolution are 60 K and 0.0067 μm. The standard deviation of the spectral fit is 0.048.

averaged at 60 K. However, since Hönl–London scaling applies (no spin uncoupling), these Einstein coefficients are equivalent to the rotationless Einstein coefficients of the molecule, and are independent of temperature to at least 600 K as shown by Billingsley.[6] The observed ratios for all the data, and average values for each v', are tabulated in Table I. The uncertainties given in Table I are statistical errors determined for the fitting and averaging procedures, and do not incorporate the systematic uncertainty of the relative response calibration.

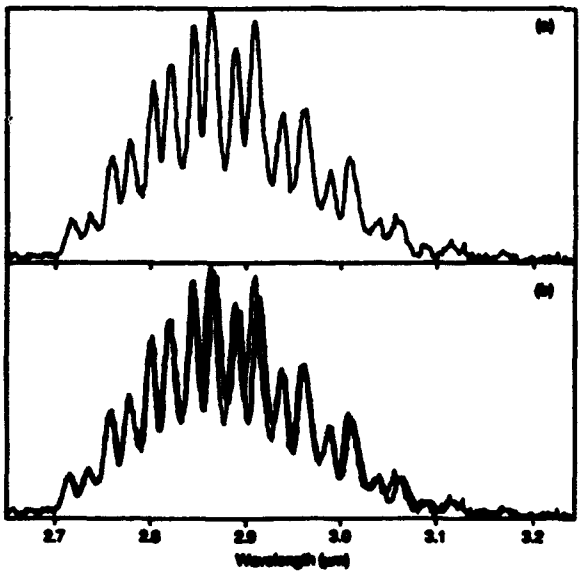

FIG. 5. Data (light line shown with the best fit and separately above) and least-squares fit (dark line) to NO($\Delta v = 2$) emission spectrum. Rotational temperature and spectral resolution are 60 K and 0.0067 μm. The slight mismatches near 2.9 and 3.1 μm result from nonlinearity in the cryogenic grating drive. The standard deviation of the spectral fit is 0.15.

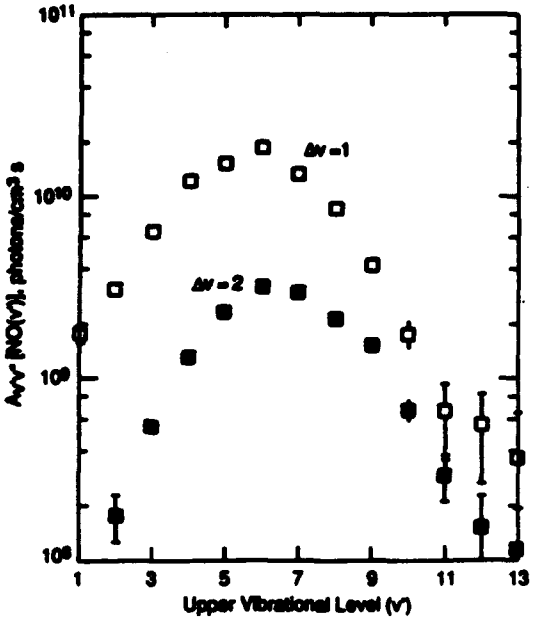

FIG. 6. Vibrational band intensities determined from a least-squares fit of fundamental and overtone spectra. Error bars denote $\pm 1\sigma$ standard deviation.

TABLE I. Experimental $(\Delta v = 2)/(\Delta v = 1)$ branching ratios.

v'	$A_{v',v'-2}/A_{v',v'-1}$ ($\pm 1\sigma$)	Weighted average ($\pm 1\sigma$)
2	0.041 ± 0.017	0.037 ± 0.001
	0.031 ± 0.026	
	0.036 ± 0.011	
	0.036 ± 0.016	
3	0.060 ± 0.011	0.078 ± 0.007
	0.084 ± 0.016	
	0.086 ± 0.009	
	0.096 ± 0.020	
4	0.096 ± 0.007	0.103 ± 0.003
	0.107 ± 0.008	
	0.107 ± 0.005	
	0.096 ± 0.010	
5	0.131 ± 0.006	0.136 ± 0.008
	0.120 ± 0.006	
	0.152 ± 0.005	
	0.131 ± 0.009	
6	0.152 ± 0.006	0.158 ± 0.007
	0.146 ± 0.006	
	0.172 ± 0.004	
	0.147 ± 0.008	
7	0.193 ± 0.008	0.202 ± 0.012
	0.215 ± 0.010	
	0.221 ± 0.007	
	0.165 ± 0.010	
8	0.202 ± 0.011	0.214 ± 0.014
	0.215 ± 0.015	
	0.247 ± 0.012	
	0.180 ± 0.016	
9	0.295 ± 0.034	0.315 ± 0.022
	0.331 ± 0.042	
	0.359 ± 0.031	
	0.263 ± 0.036	
10	0.289 ± 0.066	0.293 ± 0.027
	0.258 ± 0.063	
	0.378 ± 0.074	
	0.263 ± 0.075	
11	0.380 ± 0.234	0.384 ± 0.029
	0.319 ± 0.197	
	0.439 ± 0.222	
	0.425 ± 0.265	
12	0.387 ± 0.357	0.286 ± 0.030
	0.315 ± 0.353	
	0.279 ± 0.204	
	0.223 ± 0.267	
13	0.572 ± 0.732	0.262 ± 0.088
	0.298 ± 1.001	
	0.318 ± 0.345	
	0.082 ± 0.406	

IV. DISCUSSION

A. Comparisons to previous data

The equations relating Einstein emission coefficients to the dipole moment function are discussed in detail by Billingsley.[6] The band Einstein coefficients $A_{v',v''}$ represent thermal averages, for a given rotational temperature, of the individual state-specific Einstein coefficients for a given vibrational transition. These state-specific Einstein coefficients are proportional to the square of the dipole moment integral connecting the two states,

$$\left| \int_0^\infty \psi'(r)\mu(r)\psi''(r)dr \right|^2,$$

where $\psi'(r)$ and $\psi''(r)$ are the wave functions of the upper and lower states and $\mu(r)$ is the dipole moment as a function of internuclear distance r. For an electrically harmonic system, where $\mu(r)$ is linear, the magnitudes of the $\Delta v = 1$ transition probabilities are determined from the first derivative of the dipole moment function, while those for the overtone transitions are determined solely by the mechanical anharmonicity of the system, i.e., the nonorthogonality of the wave functions ψ' and ψ''. As the dipole moment function acquires curvature, increases in the second and third derivatives strongly increase the overtone transition probabilities. In the case of OH($X\,^2\Pi$), the dipole moment function is strongly curved near equilibrium internuclear separation, and as a result the $\Delta v = 2$ Einstein coefficients exceed those for $\Delta v = 1$ at unusually low v'.[26-30]

For NO($X\,^2\Pi$), the dipole moment function is small and only mildly curved near equilibrium separation.[2-4] Thus we expect the $\Delta v = 1$ Einstein coefficients to be primarily sensitive to the slope of $\mu(r)$, and fairly insensitive to its shape. The scaling of $A_{v',v'-1}$ with v' should be close to harmonic (i.e., $\propto v'$) near the bottom of the potential well, and will tail off at higher v' due to the increasing effects of mechanical anharmonicity in the wave functions. In addition, increasing curvature in $\mu(r)$ at large r will affect the $\Delta v = 1$ values at some high (but unknown) v'. In contrast, even modest curvature in $\mu(r)$ will profoundly affect the absolute values and v' scaling of the $\Delta v = 2$ Einstein coefficients. Thus the measurement of $(\Delta v = 2)/(\Delta v = 1)$ branching ratios over a wide range of v' provides information on the curvature of the dipole movement function over a large range of r.

The average $(\Delta v = 2)/(\Delta v = 1)$ ratios are plotted in Fig. 7, together with previously measured and predicted values. The agreement with Green *et al.*[8] is excellent over the range $4 < v' < 7$, where their data have reasonable precision. The COCHISE measured values deviate significantly from the Billingsley scaling at both low and high v', and indicate the presence of a broad maximum near $v' = 11$. The existence of such a maximum could have significant implications for the shape of the dipole moment function at large internuclear separation and for the behavior of $A_{v',v''}$ at high v' and/or J'. Unfortunately, due to the limited precision (low signal/noise) of our spectra in this region, we cannot obtain sufficiently accurate $v' = 13$ data to define the apparent downturn in the ratios for $v' > 12$. Nevertheless, the data clearly show significant deviations from the shape of the *ab initio* dipole moment function for both equilibrium and large internuclear separations.

The ratio values in Table I are appropriate for rotational temperatures below $\simeq 100$ K, and are probably reliable for temperatures up to at least 300 K. Billingsley[5,6] found that the individual line strengths departed only slightly from Hönl–London scaling, and as a result the thermally averaged Einstein coefficients were virtually independent of temperature up to 600 K. The extension of these values to higher J' and temperature requires further investigation. At some

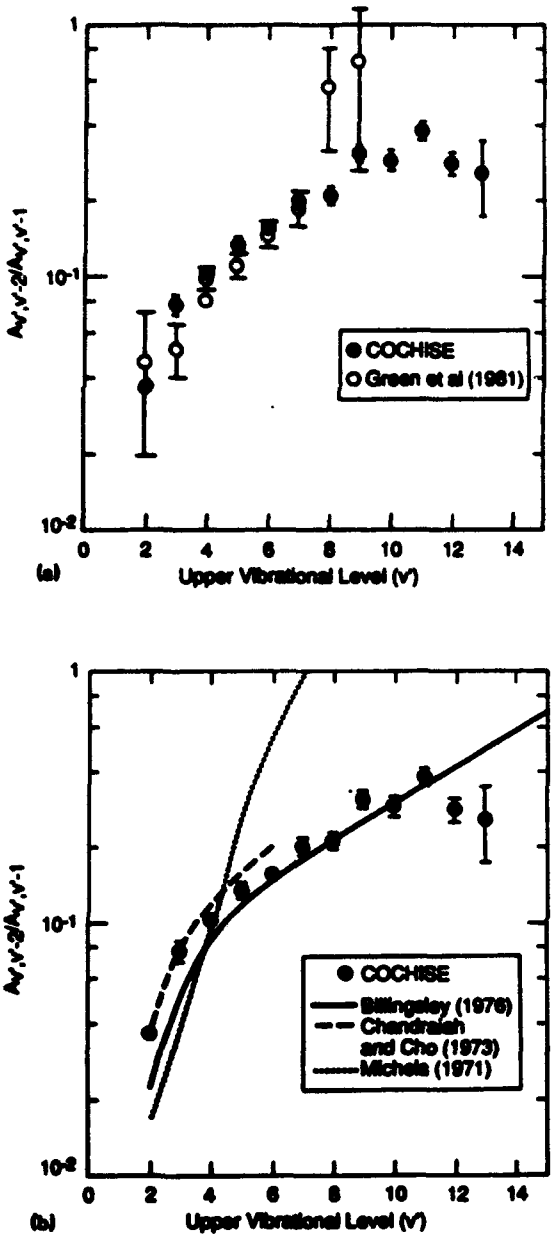

FIG. 7. Comparison of experimental branching ratios to (a) previous measurements and (b) predictions from dipole moment functions. Solid circles: weighted averages from Table I, with error bars signifying $\pm 1\sigma$ standard deviation from the weighted mean. Open circles: data from Green *et al.*, Ref. 8. Solid curve: Billingsley, Ref. 6. Dashed curve: Chandraiah and Cho, Ref. 2 (calculated in Ref. 6). Dotted curve: Michels, Ref. 1 (calculated in Ref. 6).

temperature, $A_{v'v''}$ will become sensitive to rotational distribution, since the scaling of $A(J')$ diverges from Hönl–London as J' increases.[5] It is possible that the high-J distributions resulting in R-branch band heads[11] are significantly affected, since the effects of spin-uncoupling and vibration–rotation interactions may be substantial, and further since these states sample the extremes of internuclear separation where curvature in the dipole moment function is more pronounced. Further analysis of the COCHISE data to infer an empirical dipole moment function, examine high-J effects, and compute $A_{v'v''}(T)$ will be reported elsewhere.[17]

B. Absolute Einstein coefficients: $A_{1,0}$ and $A_{2,0}$

Most of the experimental data base on NO(v) transition probabilities comes from absorption measurements on the (1,0) and (2,0) transitions. A list of previously published experimental and theoretical values for the absorption strengths and Einstein coefficients for these transitions is given in Table II. The measurements for the (1,0) transition fall into three groups: those with $A_{1,0} \approx 13$–$14\ s^{-1}$, those with 12–13, and a few early measurements of 7–8. The work of Holland *et al.*,[10] together with the extrapolated line-by-line data of Mandin *et al.*[9] as reported by Rothman *et al.*,[7] give consistent values of $A_{1,0}$ of 13.6 and $13.3\ s^{-1}$, respectively. A discussion comparing these values to previous measurements can be found in Holland *et al.*[10] In brief, the high spectral resolution and higher measurement precision of Refs. 9 and 10 indicate a significant discrepancy with the previous lower values, and strongly support a value for $A_{1,0}$ between 13 and $14\ s^{-1}$. Indeed, Rothman *et al.*[7] invoked the extrapolated line-by-line data of Mandin *et al.*[9] in their compilation of atmospheric line absorption parameters. We have adopted the value $A_{1,0} = 13.4\ s^{-1}$ at 300 K. This value is further supported by recent shock tube measurements of spectrally resolved NO($\Delta v = 1$) emission between 800 and 2500 K, which give $A_{1,0} = 13.2\ s^{-1}$ ($\pm 10\%$).[31]

The (2,0) transition probability is less well determined. Experimental values range from 0.8 to $1.1\ s^{-1}$. The most careful measurements are those of Chandraiah and Cho,[2] whose empirical dipole moment function provides good agreement with the COCHISE branching ratios at low v' (see Fig. 7). We note, however, that their result for the (1,0) band appears to be about 10–12% low.

The COCHISE data give an accurate value of $A_{2,0}/A_{2,1}$ ($\pm 2\sigma = 7.9\%$, cf. Table I), which can be used to determine $A_{2,0}$ with good precision. Billingsley[6] gives the ratio $A_{2,1}/A_{1,0} = 1.90$, 1.89, and 1.92 for the dipole moment functions of Refs. 4, 2, and 1, respectively. Since the dipole moment function is nearly linear near equilibrium internuclear separation, this particular ratio is dominated by the mechanical anharmonicity of NO (i.e., the radial wave functions for $v = 0$, 1, 2), and is relatively independent of the details of slope and shape of the dipole moment function. Thus the $A_{2,1}/A_{1,0}$ ratio is ≈ 1.9 for three very different dipole moment functions, and is probably quite accurate. We can then determine from the experimental data the ratio $A_{2,0}/A_{1,0} = 0.070$, which is identical to that determined by Chandraiah and Cho[2] and about 1.6 times that computed by Billingsley.[6] {In comparison, the experimental value for this ratio is 2.4 times larger than for the electrically harmonic [linear $\mu(r)$] case.} Application of our recommended value for $A_{1,0}$ gives the determination

$$A_{2,0} = 0.94 \pm 0.11\ s^{-1},$$

where the indicated error is the systematic uncertainty in the

TABLE II. Absorption coefficients and Einstein coefficients for the $\Delta v = 1$ and $\Delta v = 2$ transitions of NO.

Investigator	Citation	$S(0\text{–}1)$ $cm^{-2}\,Atm^{-1}$	$S(0\text{–}2)$ $cm^{-2}\,Atm^{-1}$	$A(1\text{–}0)$ s^{-1}	$A(2\text{–}0)$ s^{-1}
Havens (1938)	Ph.D. Dissertation, U. of Wisconsin	121		12.0	
Dinsmore and Crawford (1949)	U. of Minnesota Report No. NR-019-104	145 ± 29		14.3 ± 2.9	
Dinsmore (1949)	Ph.D. thesis, U. of Minnesota		2.57 ± 0.51		1.0 ± 0.2
Penner and Weber (1953)	J. Chem. Phys. 21, 649	70 ± 7	2.3 ± 0.6	6.9 ± 0.7	0.9 ± 0.2
Vincent-Geisse (1954)	Compt. Rend. 239, 251	82		8.1	
Breene (1958)	J. Chem. Phys. 28, 11; 29, 512	70	2.7	6.9	1.1
Schurin and Clough (1963)	J. Chem. Phys. 38, 1855	111 ± 7		11.0 ± 0.7	
Breene and Ferrieo (1964)	J. Chem. Phys. 41, 3420	76 ± 7	2.8 ± 0.5	7.5 ± 0.7	1.1 ± 0.2
James (1964)	J. Chem. Phys. 40, 762	138 ± 6		13.6 ± 0.6	
Fukuda (1965)	J. Chem. Phys. 42, 521	74 ± 4		7.3 ± 0.4	
Ford and Shaw (1965)	Appl. Opt. 4, 1113	115 ± 9		11.4 ± 0.9	
Alamichel (1966)	J. Phys. (Paris) 27, 345	132 ± 3		13.0 ± 0.3	
Schurin and Ellis (1966)	J. Chem. Phys. 45, 2528		2.11 ± 0.1		0.82 ± 0.04
Varanasi and Penner (1967)	J. Quant. Spectrosc. Radiat. Transfer 7, 279	128 ± 10		12.6 ± 1.0	
Oppenheim *et al.* (1967)	Appl. Opt. 6, 1305	125 ± 8		12.4 ± 0.8	
Feinberg and Camac (1967)	J. Quant. Spectrosc. Radiat. Transfer 7, 581	124 ± 22		12.3 ± 2.2	
Green and Tien (1970)	J. Quant. Spectrosc. Radiat. Transfer 10, 805	125		12.4	
Michels (1971)	Ref. 1	134 ± 2	2.0 ± 0.6	13.2 ± 0.2	0.78 ± 0.23
King and Crawford (1972)	J. Quant. Spectrosc. Radiat. Transfer 12, 443	135 ± 5		13.3 ± 0.5	
Chandraiah and Cho (1973)	Ref. 2	121 ± 6	2.17 ± 0.11	12.0 ± 0.6	0.84 ± 0.04
Garside *et al.* (1976)	Appl. Opt. 16, 398	124 ± 9		12.3 ± 0.9	
Billingsley (1976)	Ref. 6	113.3	1.31	10.78	0.46
Kunimori *et al.* (1977)	J. Quant. Spectrosc. Radiat. Transfer 19, 127	122 ± 6		12.1 ± 0.6	
Mandin *et al.* (1980)	Ref. 7, 9	134.4		13.3	
Holland *et al.* (1980)	Ref. 10	137.3 ± 4.6		13.6 ± 0.5	

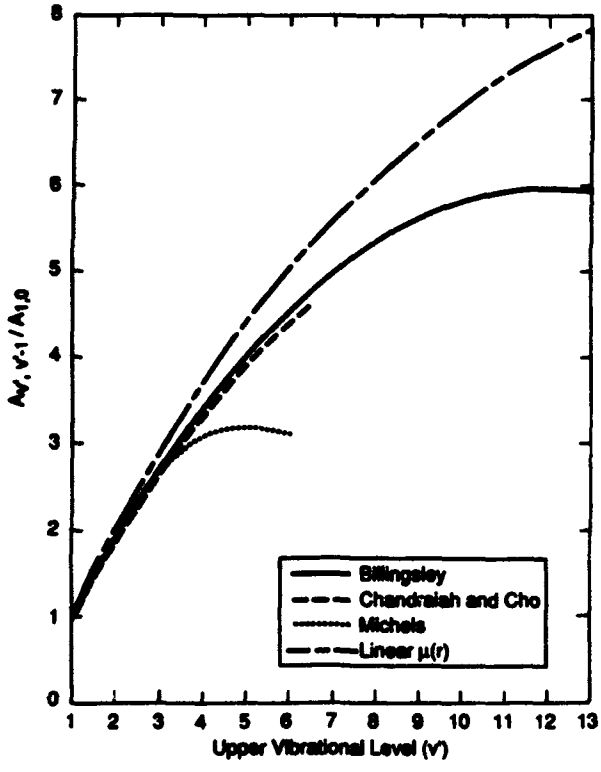

FIG. 8. Relative scaling of $\Delta v = 1$ Einstein coefficients with v'. Solid curve: Billingsley, Ref. 6. Dashed curve: Chandraiah and Cho, Ref. 2 (calculated in Ref. 6). Dotted curve: Michels, Ref. 1 (calculated in Ref. 6). Dash/dot curve: computed for a linear dipole moment function.

relative response calibration. This value is 12% higher than (but within experimental uncertainty of) that measured by Chandraiah and Cho,[2] and is a factor of 2 larger than predicted from the dipole moment function of Billingsley.[6] The relatively large value for $A_{2,0}$ indicates that the dipole moment function has more curvature near equilibrium internuclear separation than was predicted from the *ab initio* theory.

Potentially, the assumption of Billingsley scaling of $A_{v',v'-1}$ can be used with the COCHISE data to infer $A_{v',v'-2}$ values to higher v'; however, this procedure will have increasing uncertainty at higher v' as curvature in the dipole moment function plays more of a role in the v' dependence of $A_{v',v'-1}$. To evaluate the validity of this procedure, we examine the predicted $A_{v',v'-1}$ scalings as shown in Fig. 8. Predictions for the dipole moment functions of Refs. 1, 2, and 4 were taken from Ref. 6. In addition, we have plotted the predicted scaling for a linear dipole moment function as computed using Rice–Ramsperger–Kassel (RKR) wave functions for NO($X^2\Pi$). (While the absolute values of $A_{v',v'-1}$ depend on the assumed slope of $\mu(r)$, the relative values $A_{v',v'-1}/A_{1,0}$ do not.) It is clear from Fig. 7 that the relative A factors for the fundamental band are fairly insensitive to modest variations in $\mu(r)$ curvature for $v'<4$. Furthermore, the close agreement between our $A_{2,0}/A_{1,0}$ ratio and that of Chandraiah and Cho,[2] together with the similarity in v' scaling of the A factors for $\Delta v = 1$ computed by Billingsley[6] from the *ab initio*[4] and empirical[2] dipole moment functions, suggest that the Billingsley scaling is indeed reliable, at least up to $v' = 6$.

With the caveat that curvature in $\mu(r)$ at large r can affect the $A_{v',v'-1}/A_{1,0}$ scaling at high v, we tentatively conclude that Billingsley scaling is a good approximation for the fundamental band, with an uncertainty increasing with v' to perhaps $\pm$ 20% near $v' = 12$. (However, we note that there is no firm basis for extending this scaling to higher v', say $v' = 20$.) Accordingly, we have applied this scaling of $A_{v',v'-1}$ to estimate values for $A_{v',v'-2}$ using a quartic least-squares fit to the branching ratio data of Table I. The results are listed in Table III. Given the combined uncertainties in the branching ratio measurements and the $A_{v',v'-1}$ scaling, we conservatively estimate uncertainties in $A_{v',v'-2}$ ranging from $\pm$ 12% for $v' = 2$ to $\pm$ 40% for $v' = 13$.

TABLE III. Einstein coefficients for NO($\Delta v = 2$) transitions.

v'	$A_{v',v'-2}$, s^{-1} Estimated from COCHISE	*Ab initio* (Ref. 6)
2	0.94 ($\pm$ 12%)	0.46
3	2.74	1.51
4	4.8	3.10
5	7.1	4.90
6	9.8	7.29
7	13.0	9.63
8	16.6	12.50
9	20.2	15.68
10	23.9	19.14
11	26.5	22.94
12	27.9	27.15
13	27.2 ($\pm$ 40%)	31.88

V. SUMMARY AND CONCLUSIONS

We have used the infrared chemiluminescence technique, in a cryogenic reaction vessel, to measure the overtone/fundamental branching ratios for vibrational emission from NO($X^2\Pi$,v). A combination of low rotational temperature and high spectral resolution eliminated complications of non-Boltzmann rotational distributions, and minimized spectral overlap between adjacent bands. The spectral resolution also reduced complications in the analysis due to interference from other radiating species. The measurements cover ranges of 2–13 in v' and 0–12 in v'', and extend the previous experimental data base to both lower and higher vibrational levels. The agreement with predictions from a previous *ab initio* calculation is generally favorable, but detailed comparison indicates significant differences in slope and curvature of the dipole moment function at equilibrium and large internuclear separations. These differences will affect the magnitudes and v' scaling of the $\Delta v = 1$ and $\Delta v = 2$ Einstein coefficients, the more significant effect being on the overtone transitions. An experimental value derived for $A_{2,0}$ agrees with previous determinations and shows the theoretical value to be a factor of 2 too low. Further details of these effects, as well as the scaling of transition strengths for high vibrational and rotational excitation, must be addressed through derivation of an empirical dipole moment function.

ACKNOWLEDGMENTS

The authors are grateful to J. C. Person, B. D. Green, L. G. Piper, and G. E. Caledonia for informative technical discussions, and to H. C. Murphy and D. Sinclair for assistance with the laboratory experiments. The work was performed under Contract No. F19628-88-C-0173 with the Air Force Geophysics Laboratory, and was sponsored by the U.S. Air Force Office of Scientific Research under Task 2310G4 and by the Defense Nuclear Agency under Project SA, Task SA, Work Unit 115.

[1] H. H. Michels, J. Quant. Spectrosc. Radiat. Transfer 11, 1735 (1971).
[2] G. Chandraiah and C. W. Cho, J. Mol. Spectrosc. 47, 134 (1973).
[3] F. P. Billingsley II, J. Chem. Phys. 62, 864 (1975).
[4] F. P. Billingsley II, J. Chem. Phys. 63, 2267 (1975).
[5] F. P. Billingsley II, AFCRL-TR-75-0586, Air Force Geophysics Laboratory, Hanscom AFB, MA 01731, 13 Nov 1975.
[6] F. P. Billingsley II, J. Mol. Spectrosc. 61, 53 (1976).
[7] L. S. Rothman, A. Goldman, J. R. Gillis, R. R. Gamache, H. M. Pickett, R. L. Poynter, N. Husson, and A. Chedin, Appl. Opt. 22, 1616 (1983).
[8] B. D. Green, G. E. Caledonia, and R. E. Murphy, J. Quant. Spectrosc. Radiat. Transfer 26, 215 (1981).
[9] J. Y. Mandin, C. Amiot, and G. Guelachvili, Ann. Phys. (Paris) 5, 91 (1980).
[10] R. F. Holland, M. C. Vásquez, W. H. Beattie, and R. S. McDowell, J. Quant. Spectrosc. Radiat. Transfer 29, 435 (1983).
[11] W. T. Rawlins, M. E. Fraser, and S. M. Miller, J. Phys. Chem. 93, 1097 (1989).
[12] J. P. Kennealy, F. P. Del Greco, G. E. Caledonia, and B. D. Green, J. Chem. Phys. 69, 1574 (1978).
[13] G. E. Caledonia and J. P. Kennealy, Planet. Space Sci. 30, 1043 (1982).

[14] W. T. Rawlins, G. E. Caledonia, J. J. Gibson, and A. T. Stair, Jr., J. Geophys. Res. **86**, 1313 (1981).
[15] D. E. Siskind, C. A. Barth, and R. G. Roble, J. Geophys. Res. **94**, 16885 (1989).
[16] R. H. Picard, J. R. Winick, R. D. Sharma, A. S. Zachor, P. J. Espy, and C. R. Harris, Adv. Space Res. **7**, 23 (1987).
[17] W. T. Rawlins, J. C. Person, M. E. Fraser, and W. A. M. Blumberg, J. Chem. Phys. (submitted).
[18] W. T. Rawlins, H. C. Murphy, G. E. Caledonia, J. P. Kennealy, F. X. Robert, A. Corman, and R. A. Armstrong, Appl. Opt. **23**, 3316 (1984).
[19] M. E. Fraser, W. T. Rawlins, and S. M. Miller, J. Chem. Phys. **92**, 1758 (1990).
[20] W. T. Rawlins and R. A. Armstrong, J. Chem. Phys. **87**, 5202 (1987).
[21] W. T. Rawlins, G. E. Caledonia, and R. A. Armstrong, J. Chem. Phys. **87**, 5209 (1987).
[22] M. E. Fraser, W. T. Rawlins, and S. M. Miller, J. Chem. Phys. **88**, 538 (1988).
[23] W. T. Rawlins, A. Gelb, and R. A. Armstrong, J. Chem. Phys. **82**, 681 (1985).
[24] A Goldman and S. C. Schmidt, J. Quant. Spectrosc. Radiat. Transfer **15**, 127 (1975).
[25] G. Herzberg, *Molecular Spectra and Molecular Structure: I. Spectra of Diatomic Molecules* (Van Nostrand, Toronto, 1950).
[26] S. R. Langhoff, H. J. Werner, and P. Rosmus, J. Mol. Spectrosc. **118**, 507 (1986).
[27] D. N. Turnbull and R. P. Lowe, J. Chem. Phys. **89**, 2763 (1988).
[28] D. D. Nelson, Jr., A. Schiffman, D. J. Nesbitt, and D. J. Yaron, J. Chem. Phys. **90**, 5443 (1989).
[29] D. D. Nelson, A. Schiffman, and D. J. Nesbitt, J. Chem. Phys. **90**, 5455 (1989).
[30] D. D. Nelson, Jr., A. Schiffman, and D. J. Nesbitt, J. Chem. Phys. **93**, 7003 (1990).
[31] W. T. Rawlins, R. R. Foutter, and T. E. Parker (in preparation).

Quenching of $N(^2D)$ by $O(^3P)$

C. Fell and J. I. Steinfeld
Department of Chemistry, Massachusetts Institute of Technology, Cambridge, Massachusetts 02139
S. Miller
Air Force Geophysics Laboratory, Bedford, Massachusetts 01731

(Received 28 September 1989; accepted 28 November 1989)

A definitive measurement of the rate coefficient for the quenching of $N(^2D)$ by $O(^3P)$ is reported. The $O(^3P)$ atoms were generated by titrating NO directly into the active nitrogen flow. Analysis of the results required that the rate coefficient for the reaction $N(^2D) + NO \rightarrow N_2 + O$ be known accurately, and this was also determined. A finite mixing time correction is also necessary. The best estimate of the rate coefficient from this work is $(6.9 + 0.7, -1.1) \times 10^{-13}$ cm^3 s^{-1} at $T = 298$ K, considerably smaller than a previous measurement [J. Phys. Chem. 92, 5977 (1988)] and in much better accord with values required by atmospheric models.

I. INTRODUCTION

$N(^2D)$ is an important constituent of the mesophere and thermosphere. Atmospheric modeling studies[1-3] indicate that the reaction

$$N(^2D) + O_2 \xrightarrow{k_{1a}} NO(v) + O(^3P,^1D) \quad (1)$$

is the primary source of the NO concentrations first observed in rocket experiments.[4] While the value of the rate coefficient for reaction (1) is well established,[5-10] the coefficient for the quenching reaction

$$N(^2D) + O(^3P) \xrightarrow{k_Q} N(^4S) + O(^3P) \quad (2)$$

is still the subject of some dispute. The relative magnitude of these two rate coefficients is important in determining the partitioning between the two product channels. Modeling calculations require that reaction (1) be the dominant loss channel for $N(^2D)$. A recent experimental measurement[11] of the rate coefficient for reaction (2) reported a value of $3.4 \times 10^{-11} \times \exp(-145/T)$ cm^3 s^{-1}, which would correspond to 2.1×10^{-11} cm^3 s^{-1} at $T = 300$ K; the quoted error limits are on the order of $\pm 50\%$. This value is considerably higher than previous determinations and more discordant with preferred modeling values[2,12-15] which require $k_Q < 10^{-12}$ cm^3 s^{-1}. If this rate were correct, then $N(^2D)$ would contribute to the overall depletion of NO by enhancing the $N(^4S)$ concentration which reacts rapidly with NO through the reaction

$$N(^4S) + NO \xrightarrow{k_N} N_2 + O(^3P). \quad (3)$$

This would necessitate a re-evaluation of the role of $N(^2D)$ in the upper atmosphere and the identification of another source term for NO.

We have remeasured the rate coefficients for both reactions (1) and (2) in order to establish the true partitioning between these two $N(^2D)$ loss channels. This was done using the FACELIF reactor[16] with multiphoton ionization (MPI) detection of reactant and product species. The experimental method makes use of reaction (3) to generate the $O(^3P)$ atom quenchers.[11] As this reaction takes place directly in the main flow, recovery of k_Q requires that the rate coefficient for the reaction

$$N(^2D) + NO \xrightarrow{k_{NO}} N_2 + O \quad (4)$$

be known accurately. Reported values[17,18] for this rate coefficient range from 5.9×10^{-11} to 1.8×10^{-10} cm^3 s^{-1}; thus, it was necessary to carry out a measurement of k_{NO} as well, in order to determine the correct value of k_Q.

II. EXPERIMENTAL

A. Apparatus

The experimental setup was essentially the same as that used in previous rate measurements performed using the FACELIF reactor[16] and will therefore be described only briefly here. A schematic is shown in Fig. 1. The $N(^2D)$ atoms were produced in a 70 W microwave discharge of a 1%–2% mixture of N_2 in helium. The N_2 and He were purified using gettering furnaces containing Cu at 600 °C and Ti at 800 °C, respectively, to remove O_2 impurities prior to entering the discharge tube. The NO (Matheson 98% purity) was flowed through a purifying manifold consisting of an ascarite trap and a liquid nitrogen/methanol slurry, and was then diluted with He to ~10% concentration prior to use. All other quenchers were used without furthur purification.

Metastable nitrogen atoms are deactivated at essentially every wall collision.[6,19] The $N(^2D)$ concentrations created by microwave discharges are approximately two orders of magnitude lower than the ground state nitrogen atom concentration. The combination of these two factors made it essential, under certain circumstances, to be able to introduce the metastable atoms into the reaction zone as quickly as possible, while the $N(^2D)$ was still in sufficient concentration to provide an adequate signal level. This necessitated a fast pumping speed which was provided by a Rootes blower (Leybold–Heraeus WS1000) backed by a large displacement forepump (Heraeus–Englehard DK180). The maxi-

 0021-9606/90/084768-10$03.00

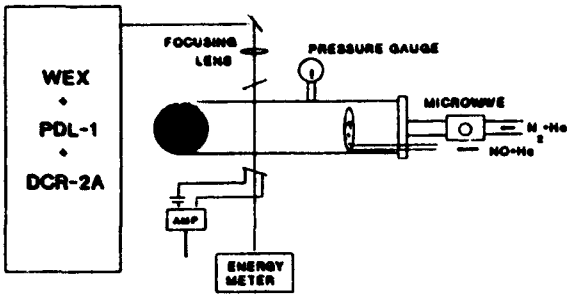

FIG. 1. Schematic of FACELIF experimental apparatus. The solid circle represents a right angle connection to the pumping system.

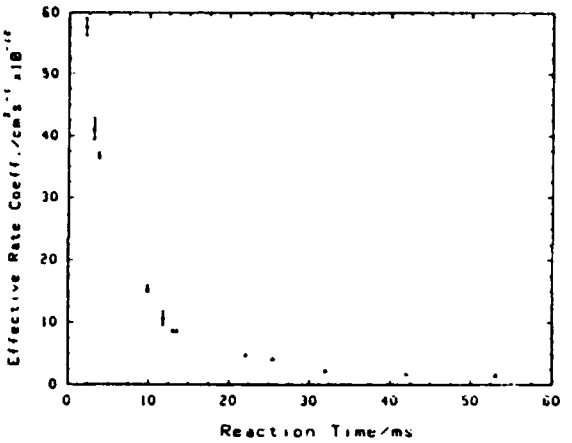

FIG. 2. Variation in the effective rate coefficient, k_{eff} [Eq. (5)] with reaction time. The reaction time was varied by adjustments to the injector position and the flow speed. Consequently, the flow conditions [i.e., total pressure, [N(^4S)] etc.] varied with the reaction time.

mum linear flow velocity attainable using this configuration was of the order of 6000 cm s^{-1}, which corresponds to a minimum flow time of approximately 2 ms. Longer flow times could be achieved by reducing the pumping speed as required. Quenching gases were injected through a loop injector whose position could be adjusted, over a limited range, along the length of the flow tube, again altering the flow time. Some comparative studies were performed using a perforated ball injector to probe any possible disparities in mixing properties. These indicated that the mixing characteristics were comparable with marginally poorer mixing for the ball injector.

The N(^2D) concentration was monitored using resonance enhanced multiphoton ionization.[18,19] The frequency doubled output of a Nd:YAG pumped dye laser (Quanta-Ray DCR2A, PDL-1, WEX-1) was used to photoionize N(^2D), resonantly enhanced by the two-photon transitions at 268.95 and 268.98 nm.[20] The current produced across a pair of Ni wire grids, biased at 90 V, was amplified using an Ithaco model 1211 current preamplifier and averaged on an EG & G model 162 boxcar averager. Signal levels were generally measured by setting the laser on resonance at each data point and subtracting the off-resonance baseline from the averaged signal. Some results were also taken by scanning the laser across the resonance lines with no significant difference in the results.

The method used to generate the O(^3P) quenchers involves the titration of NO directly into the flowtube.[11] The NO/He mixture is introduced into the flow, through the loop injector, where it reacts rapidly with N(^4S),[21] which is present in high concentrations in microwave discharge flows of N_2/He. Under ideal conditions, the N(^4S) will be in sufficient excess that all the NO will be rapidly converted to O(^3P) before making any significant contribution to the N(^2D) quenching. The diffusion coefficient for O atoms in He is 700 cm^2 s^{-1},[22] and the surface recombination coefficient is on the order of 10^{-4}.[23] For the flowspeeds and pressures used in our 2 in. diameter flowtube, we estimate less than 1% loss of O(^3P) over the reaction length.

B. Experimental procedure

Preliminary experiments were carried out investigating the variation in the total N(^2D) quenching rate over a wide range of reaction times. These were used to calculate an effective rate coefficient at each reaction time. This is defined as

$$k_{eff} = -\alpha(v/d)(d\ln[N(^2D)]/d[Q]), \quad (5)$$

where v is the average flow speed, d is the injector to detector distance, α is the nonlaminar flow correction having a numerical value of 1.62,[9] and [Q] is the initial quencher concentration. The use of Eq. (5) is equivalent to assuming that all the initially added NO is converted instantaneously to O(^3P) by the N(^4S) without contributing to the N(^2D) decay. The results, shown in Fig. 2, display a rapid decrease in the effective rate coefficient with increasing reaction time. Even at ~50 ms there is some indication that the rate coefficient is still approaching an asymptotic value of less than 1×10^{-12} cm^3 s^{-1}. The flow conditions over this range of reaction times necessarily varied by a substantial amount. The total pressure varied from 0.2 to 4 Torr in going from short to longer reaction times. There was a corresponding change in the N(^4S) concentration, although this was not explicitly measured for all points along the curve. The percentage of initially added NO remaining unreacted at the detection point was also measured for the same range of reaction times. The NO γ(0,0) MPI signals[24,25] were used for this purpose. The magnitude of this signal is directly proportional to the NO concentration. A blank titration was performed under the same set of experimental conditions, except with the discharge turned off. The ratio of the two slopes yields a value of the fraction of initially added NO that remains unreacted. The results are shown in Fig. 3.

Comparison of Figs. 2 and 3 shows clearly that the faster effective rate constants are correlated with significant residual NO concentrations. The short reaction time measurements represent a region in which reaction with NO dominates the N(^2D) decay. These measurements indicate an extreme lower limit on k_{NO}. The longer reaction time measurements, to the extent that there is still some NO contribu-

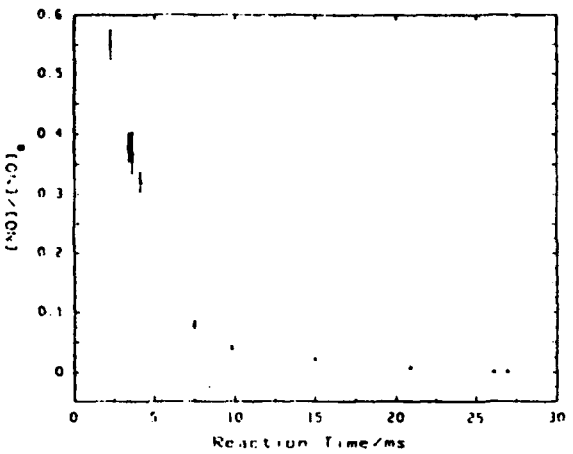

FIG. 3. Variation in the fractional amount of initially added NO that remained unreacted at the MPI-detection point. As with the k_{eff} measurements, flow conditions varied with reaction time.

tion to the effective decay rate, represent an extreme upper limit on the $O(^3P)$ quenching rate coefficient. The limiting values obtained for k_{NO} and k_O obtained in this way, indicate a ratio for these two rate coefficients in excess of 25 to 1. Consequently, for short reaction times, where $[NO] \sim [O]$, the $O(^3P)$ contribution is smaller by a factor k_O/k_{NO}, and may be legitimately neglected when determining k_{NO}. Conversely, the large value of k_{NO} compared to k_O means that even very small amounts of NO may cause a significant degree of quenching.

It has been reported that REMPI detection of $N(^2D)$ at 269 nm can generate $N(^2D)$ through the two photon dissociation of NO.[26,27] In order to ensure that this effect was not compromising our results we looked for the characteristic $N(^2D)$ signal at high NO flow with the discharge turned off (i.e., with [NO] significantly higher than normal operating conditions). No signal was observed until [NO] was over 100 times that used during titrations. The laser power, measured after exiting the flow tube, was <0.5 mJ pulse^{-1} compared to the 2–5 mJ pulse^{-1} reported by Jusinski *et al.*[26] This gives a production rate ratio of between 1:16 and 1:100 for the two systems. Also, NO concentrations in the detection region were always <0.5 mTorr. The combination of these two factors accounts for the lack of any measurable levels of $N(^2D)$ production from NO dissociation.

Measurements of k_{NO} and k_O both require knowledge of $[N(^4S)]$ to determine how fast the NO is depleted and therefore the extent to which it contributes to the $N(^2D)$ decay. For long reaction times the standard NO titration method[28] may be used to determine $[N(^4S)]$ accurately. This technique has serious limitations at the shorter reaction times to which the NO rate coefficient measurements were constrained. To obtain a distinct titration end point, reaction (3) must have sufficient time to go to completion. The method therefore, is best suited to conditions, where $[N(^4S)]$ is high and the reaction time is long. This is precisely the opposite of the requirements for accurate k_{NO} measurements. Other practical difficulties were encountered in the form of greatly reduced signal levels and interfering fluorescence. The fast flows and consequent low pressures (0.2–0.4 Torr) lead to significantly reduced signal levels and a subsequent reduction in signal to noise. In addition, stray light from the discharge created a background large in comparison to the target signal. Anomalous effects were observed for small NO additions in the form of an initial rise in signal level. It is possible that this has its origins in fluorescence resulting from some coincident reaction. It has been previously reported[29] that some short-lived source of $N_2(B)$, other than $N(^4S)$ atom recombination, exists in discharge flows which may interfere with titration measurements.

Attempts were made to fit the titration plots for short reaction times. This introduced a further limitation beyond the practical problems already mentioned. Fitting would require the use of the rate coefficient for reaction (3), which has associated error bounds that will propagate into the $[N(^4S)]$ value. As a result of these limitations, an alternative method of determining $[N(^4S)]$ was devised. Measurements of NO depletion were made using γ (0,0) MPI band intensities, as described earlier. The high sensitivity of MPI to NO enables very small concentrations to be detected and it is therefore possible to work with $[N(^4S)] \gg [NO]$. The NO decay can then be described by the pseudo-first-order rate equation

$$[NO]_t = [NO]_0 \exp(-k_N[N(^4S)]t), \quad (6)$$

where $[NO]_0$ is the initial concentration of NO added. The $N(^4S)$ concentration is simply given by

$$[N(^4S)] = -\ln\{[NO]/[NO]_0\}/(k_N t) \quad (7)$$

Since the ratio $[NO]/[NO]_0$ may be determined very precisely, the accuracy of this technique is limited by the uncertainty in k_N.

For slow flows (>20 ms), it is reasonable to assume that the mixing time is short in comparison to the total flow-time. For very fast flows (<5 ms), this assumption may lead to a significant underestimation of the rate coefficients. A standard technique used to probe mixing effects is to perform rate measurements over a range of injector positions under constant flow conditions. A plot of the decay coefficient as a function of the flowtime will give a straight line whose x-axis intercept gives a value for the effective mixing time and whose slope yields a value for the rate coefficient. In the case of NO, the accompanying reaction with $N(^4S)$ depletes NO and thus compromises the technique. In order to circumvent this problem, we performed the rate measurements substituting O_2 as a quencher. If it is assumed that the mixing characteristics for O_2 and NO are comparable, then the effective mixing time obtained using O_2 may be applied to NO, provided that identical flow conditions are employed.

III. ANALYSIS OF RESULTS

Measurements of both k_{NO} and k_O involve injecting NO molecules directly into the main discharge flow, where they react rapidly with $N(^4S)$ atoms to generate $O(^1P)$. What-

ever the flow conditions, the NO will be present for some finite time in the tube. The $N(^2D)$ atoms may be quenched by $O(^3P)$ and NO, both of which will be present in varying concentrations along the length of the flowtube. From reactions (2) and (3), the rate equation describing the decay of $N(^2D)$ is

$$\frac{-d[N(^2D)]}{dt} = k_{NO}[N(^2D)][NO] + k_O[N(^2D)][O] + k_w[N(^2D)], \quad (8)$$

where k_w is the first order rate coefficient for wall deactivation. Integration of this equation over the reaction time gives

$$-\ln\{[N(^2D)]/[N(^2D)]_0\} = k_{NO}\int_0^t [NO]dt + k_O\int_0^t [O]dt + k_w t, \quad (9)$$

where $[N(2D)]_0$ is the initial concentration of $N(^2D)$. The concentration of $O(^3P)$ at any given time is simply equal to $[NO]_r$, the amount of NO reacted, if there is no other significant loss of $O(^3P)$.

The rate of change of NO with time is given by

$$\frac{-d[NO]}{dt} = k_N[NO][N(^4S)] + k_{NO}[NO][N^*], \quad (10)$$

where $[N^*]$ is the metastable nitrogen atom concentration. Since $[N(^4S)] \gg [N^*]$, the second term in Eq. (10) may be neglected, and the NO concentration is given by Eq. (6). Substituting this into Eq. (9) gives

$$-\ln\left\{\frac{[N](^2D)}{[N(^2D)]_0}\right\} = k_O[NO]_0 t + \frac{(k_{NO}-k_O)}{k_N[N(^4S)]} \times\{1-\exp(-k_N[N(^4S)]t)\} \times[NO]_0. \quad (11)$$

For the situation where $[N(^4S)]$ cannot be considered to be in large excess, a slightly more complex expression results. The NO concentration, in this instance, is expressed as

$$\frac{-d[NO]}{dt} = k_N\{[NO]_0 - [NO]_r\} \times\{[N(^4S)]_0 - [NO]_r\}, \quad (12)$$

where $[N(^4S)]_0$ is the initial ground state nitrogen atom concentration. This is a second order rate equation which when integrated gives[6]

$$\frac{1}{([NO]_0 - [N(^4S)])}\ln\left\{\frac{[N(^4S)]}{[NO]_0}\frac{([NO]_0-[NO]_r)}{([N(^4S)]-[NO]_r)}\right\} = k_N t. \quad (13)$$

Rearranging this expression for [NO] gives

$$[NO]_r = \frac{[N(^4S)] - ([NO]_0[N(^4S)]/[NO]_0)\exp\{-([NO]_0-[N(^4S)])k_N t\}}{1-([N(^4S)]/[NO]_0)\exp\{-([NO]_0-[N(^4S)])k_N t\}}. \quad (14)$$

The $N(^2D)$ concentration at any point along the flowtube is given by

$$-\ln\left\{\frac{[N(^2D)]}{[N(^2D)]_0}\right\} = k_{NO}[NO]_0 t + (k_O - k_{NO}) \times\int_0^t [NO]dt + \text{const.} \quad (15)$$

$\int_0^{t_{max}} [NO]dt$ must be evaluated by numerical integration over the range $t = 0$ to t_{max}, where t_{max} is the reaction time corrected for mixing effects.

IV. RESULTS AND DISCUSSION

An estimate of the effective mixing time for the NO kinetic runs was obtained from the O_2 rate measurements. The results are shown in Fig. 4. The total pressure in the flowtube was ~0.4 Torr with a linear flow velocity of ~6000 cm s^{-1}. A weighted linear regression fit to the data yields a value of (0.48 ± 0.19) ms for the effective mixing time. The slope of the line in Fig. 4 gives a value of the $N(^2D) + O_2$ rate coefficient of $(5.89 \pm 0.40) \times 10^{-12}$ cm^3 s^{-1}, in good agreement with previous determinations.[5-10]

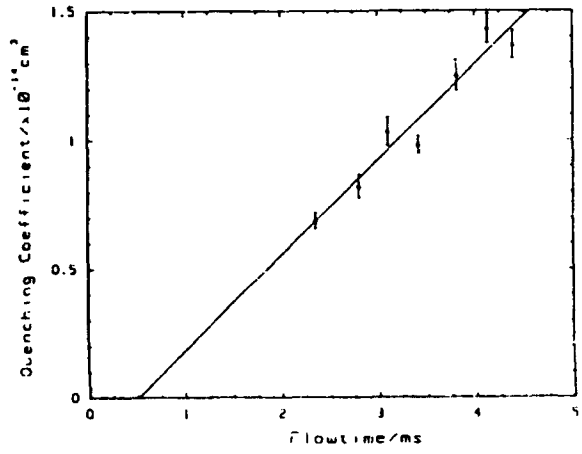

FIG. 4. Variation in the decay coefficient ($-d\ln[N(^2D)]/d[O_2]$) with reaction time for $N(^2D)$ quenching by O_2. Flowtube pressure was 0.46 Torr at a linear flow velocity of 6700 cm s^{-1}. The error bars represent the statistical limits to the decay coefficient obtained from a weighted linear regression fit to the individual data sets.

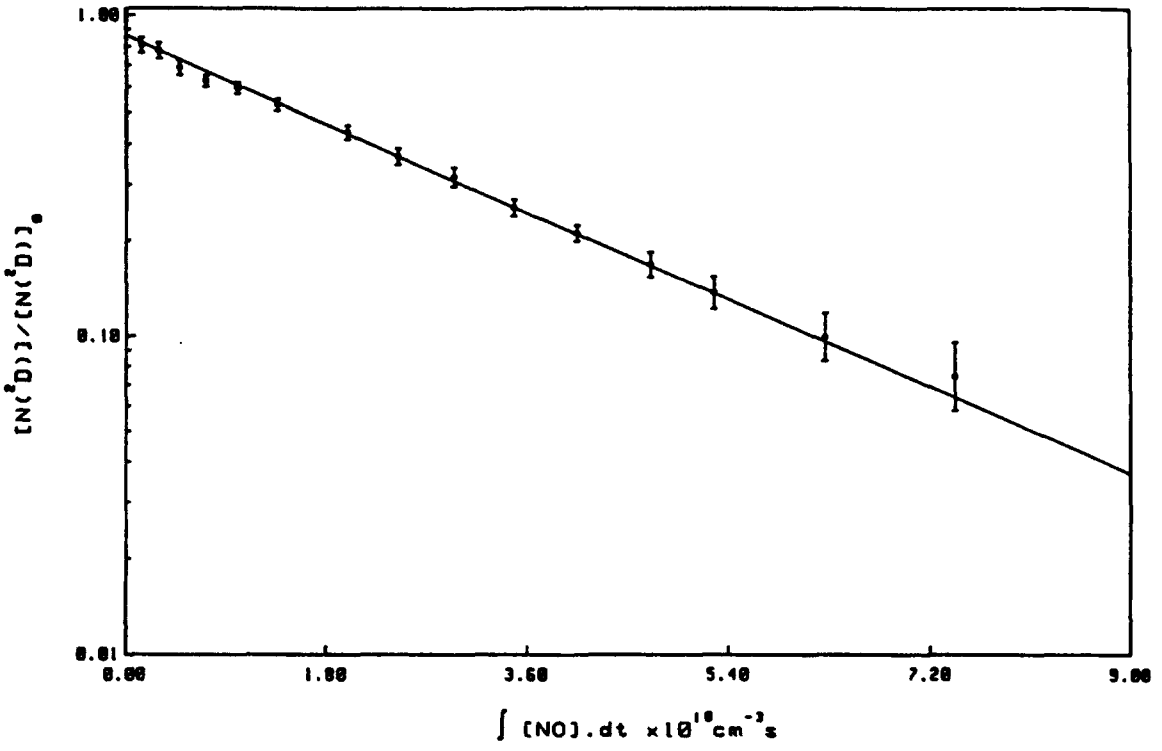

FIG. 5. Decay of the $N(^2D)$ MPI signal as a function of $\int_0^t [NO]dt$, which was calculated by numerical integration of Eq. (14). $t = 3.90$ ms (corrected for 0.48 ms mixing time), $k_N = 3.4\times10^{-11}$ cm^3 s^{-1}, and $[N(^4S)] = 0.43$ mTorr.

The NO experiments were carried out using identical flow conditions to those for the O_2 runs. The $N(^4S)$ concentrations were varied between 0.25 and 0.45 mTorr. For these conditions $\int_0^t [O]dt \sim \int_0^t [NO]dt$, but as $k_{NO} \gg k_O$, the $O(^3P)$ atom quenching may be neglected. From Eq. (9), a plot of the $N(^2D)$ signal decay vs $\int_0^t [NO]dt$ will give a straight line whose slope gives a value for k_{NO} directly. Such a plot is shown in Fig. 5 for $t = 3.90$ ms and $[N(^4S)] = 0.43$ mTorr.

There are a number of sources of error that must be considered in calculating k_{NO}. Uncertainties in signal levels are shown as error bars in Fig. 5. The dynamic range of the $N(^2D)$ decay which could be followed was limited by the appearance of the NO $\gamma(0,4)$ band at higher NO concentrations, which obscured the $N(^2D)$ signal to some extent. This baseline variation is reflected in the larger error bars for high [NO] additions. The vibrationally excited NO population is presumably the result of the reaction[30]

$$N_2(A) + NO(X) \rightarrow N_2(X) + NO(A) \qquad (16)$$

followed by γ-band emission, although this has not been confirmed experimentally.

The value used for k_N in the calculations is taken from the literature[21] and has an associated uncertainty of $\pm 26\%$. This value is used in calculating $[N(^4S)]$ and again in the integration of $\int_0^t [NO]dt$. This error manifests itself as a shift in the x-axis position of the data points. The extreme values for k_N, $[N(^4S)]$, and t_{max} were used to calculate upper and lower bounds for k_{NO}. These bounds are shown in Fig. 6 for the data shown in Fig. 5. The upper and lower bounds, together with rate coefficient obtained using the mean values of k_N, $[N(^4S)]$ and t_{max}, are given in Table I for all kinetic runs. The error limits on each value are the statistical errors ($\pm 1\sigma$) obtained from a weighted linear regression fit to the data points in each limit. These are small in comparison to the error bounds indicating that the dominant source of error arises from the uncertainty in the values of k_N and the mixing time. The final values are obtained by taking the weighted mean of all kinetic runs. This procedure yields a result of $(6.70, +1.36, -1.21)\times10^{-11}$ cm^3 s^{-1} for k_{NO}.

The ideal conditions in which to measure k_O are at long reaction times with $[NO] \ll [N(^4S)]$. If these conditions can be fulfilled then Eq. (11) may be used to evaluate k_O. Given the great disparity between k_{NO} and k_O, these conditions are extremely difficult to realize in practice. At the slowest flows, the use of high flowtube pressures was not sufficient to offset the loss of signal due to increased wall deactivation, thus constraining the experimental range of t. The maximum $[N(^4S)]$ values obtained, even under these

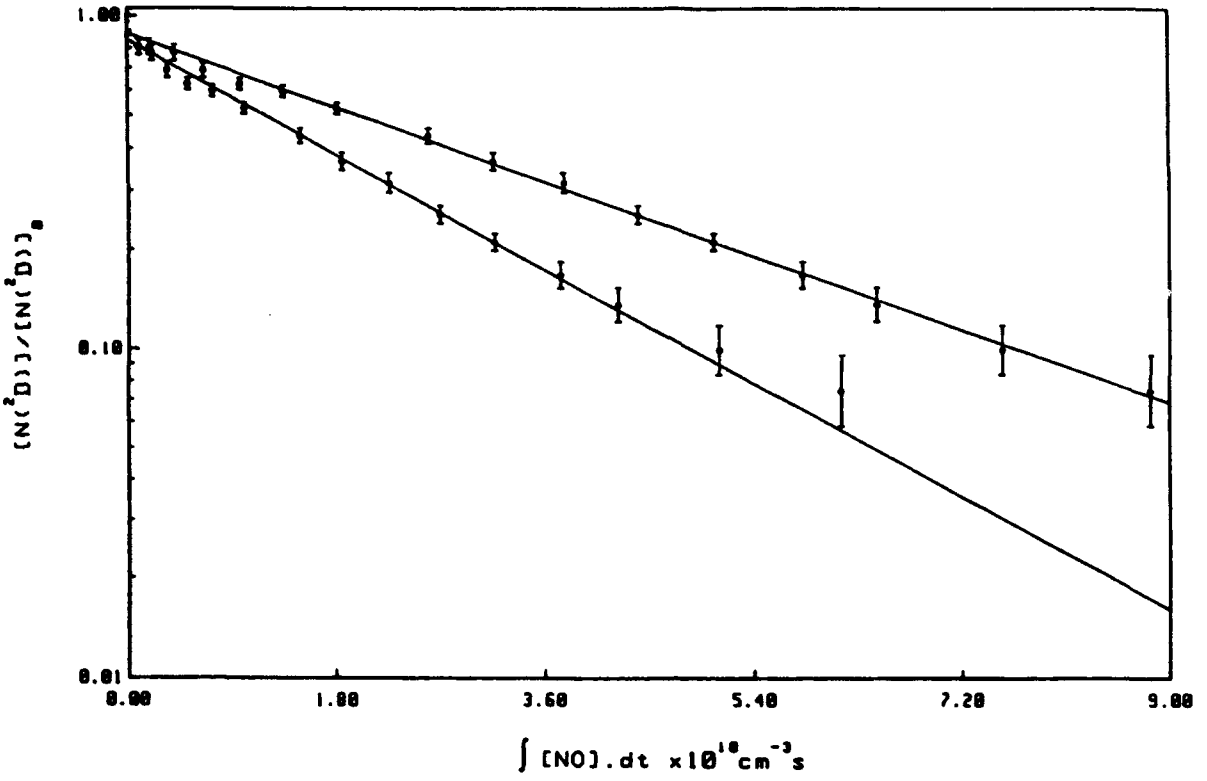

FIG. 6. Error bounds on the decay of the $N(^2D)$ MPI signal as a function of $\int_0^t [NO]dt$ for the data shown in Fig. 5. Lower trace: $t = 3.71$ ms, $k_N = 4.3 \times 10^{-11}$ cm^3 s^{-1} and $[N(^4S)] = 0.52$ mTorr. Upper trace: $t = 4.09$ ms, $k_N = 2.5 \times 10^{-11}$ cm^3 s^{-1} and $[N(^4S)] = 0.34$ mTorr.

extreme conditions, were 1.6×10^{14} cm^{-3} ($\sim$5 m Torr). The low value of k_O required NO additions of up to 3.5 mTorr to give $[N(^2D)]/[N(^2D)]_0 < 0.05$ and thus the $[N(^4S)] \gg [NO]$ condition could not be met. Some attempts were made to enhance N-atom dissociation by adding SF_6 to the discharge flow.[31] This did result in a significant increase in $[N(^4S)]$ (by a factor of up to 2.5) and also in the $N(^2D)$ signal level. Unfortunately, the use of SF_6 also resulted in the appearance of a large molecular MPI spectrum in the same frequency range which also varied with quencher concentration and therefore compromised the results. It is possible that such interferences would not occur for other $N(^2D)$ detection methods. If this were true, then this method could be used to enhance both $N(^4S)$ and $N(^2D)$, assuming that the species generated by discharging SF_6 do not participate in the chemistry in any way.

TABLE I. Kinetic data for determination of $N(^2D) + NO \rightarrow N_2 + O$ rate coefficient.

t, ms	k_{NO}, cm^3 molecule^{-1} s$^{-1} \times 10^{11}$ Lower bound	Mid range	Upper bound
1.82	6.11 ± 0.18	7.72 ± 0.22	8.79 ± 0.26
	6.65 ± 0.28	8.52 ± 0.36	9.73 ± 0.41
2.625	7.38 ± 0.31	8.77 ± 0.37	10.30 ± 0.43
	7.53 ± 0.30	8.88 ± 0.35	10.60 ± 0.42
3.175	5.81 ± 0.22	7.13 ± 0.27	8.89 ± 0.34
	6.64 ± 0.40	8.24 ± 0.50	10.40 ± 0.63
3.385	6.56 ± 0.30	7.84 ± 0.36	9.47 ± 0.43
	6.56 ± 0.26	7.76 ± 0.31	9.28 ± 0.37
3.865	4.39 ± 0.18	5.13 ± 0.22	6.06 ± 0.25
	4.61 ± 0.24	5.38 ± 0.28	6.38 ± 0.33
3.895	4.61 ± 0.13	5.67 ± 0.16	7.15 ± 0.20
	5.00 ± 0.18	6.13 ± 0.22	7.63 ± 0.27
Weighted mean	5.49 ± 0.07	6.70 ± 0.08	8.06 ± 0.10

Equation (15) was used in calculating k_O. The previously determined value of k_{NO} was used and the NO contribution to the decay subtracted at each point. Figures 7 and 8 show the effect of applying this correction to the raw data for two separate kinetic runs. The relative contribution from NO increases with increased quencher addition and shorter reaction time. Even for the highest $[N(^4S)]$ values and longest flowtimes, NO accounted for $\sim$30% of the $N(^2D)$ decay.

The $N(^4S)$ concentration can be measured by the more usual titration technique for these slow flow conditions. $[N(^4S)]$ was measured before and after each kinetic run with results agreeing to within 2% in all instances. We conservatively estimate an accuracy of $\pm$ 5% for the NO titration technique. The mixing time was not explicitly measured for these longer reaction times as this can reasonably be ex-

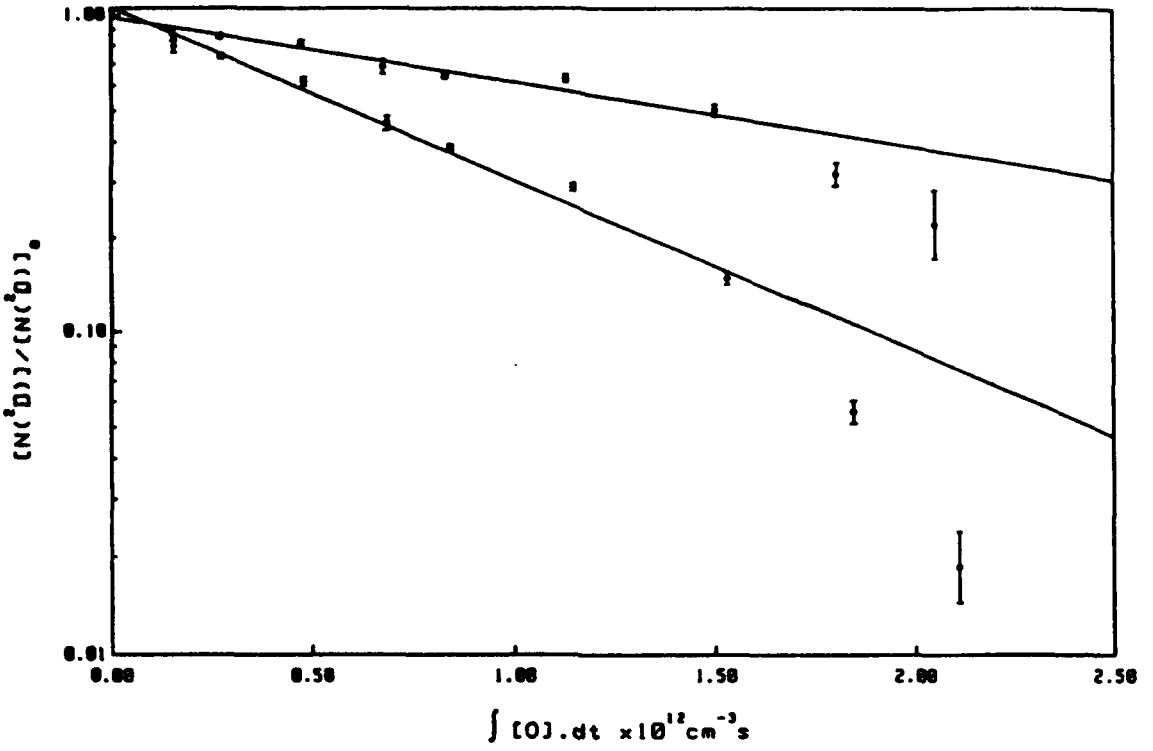

FIG. 7. Decay of the N(^2D) MPI signal as a function of $\int_0^t [O]dt$. The bottom trace was calculated assuming instantaneous conversion of [NO] to [O] (i.e., $\int_0^t [O]dt = [NO]_0 t$) and therefore no correction for depletion of N(^2D) by NO is necessary. A linear regression fit to these data gives a value of $k_O = 2.03 \times 10^{-12}$ cm^3 s^{-1}. The upper trace was calculated using Eq. (15) with $k_N = 3.4 \times 10^{-11}$ cm^3 s^{-1}, $k_{NO} = 6.7 \times 10^{-11}$ cm^3 s^{-1}, [N(^4S)] = 3.28 mTorr and $t = 23.0$ ms. This gives a value of $k_O = 7.60 \times 10^{-13}$ cm^3 s^{-1}. The difference in the two plots shows the relative magnitude of the NO contribution to the N(^2D) signal decay.

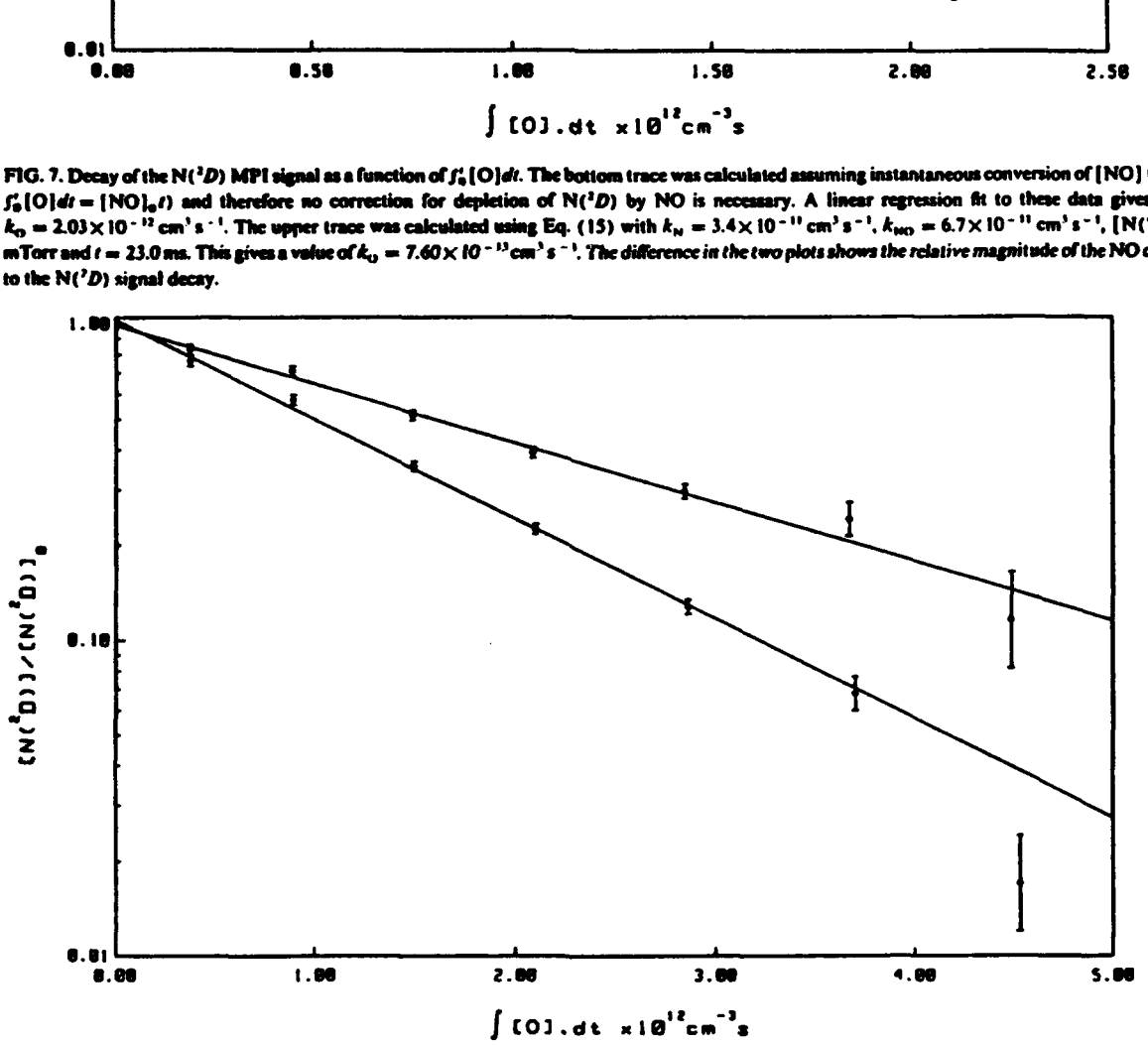

FIG. 8. Same as Fig. 7 for $t = 41.4$ ms. The top trace was calculated using $k_N = 3.4 \times 10^{-11}$ cm^3 s^{-1}, $k_{NO} = 6.7 \times 10^{-11}$ cm^3 s^{-1} and [N(^4S)] = 4.28 mTorr.

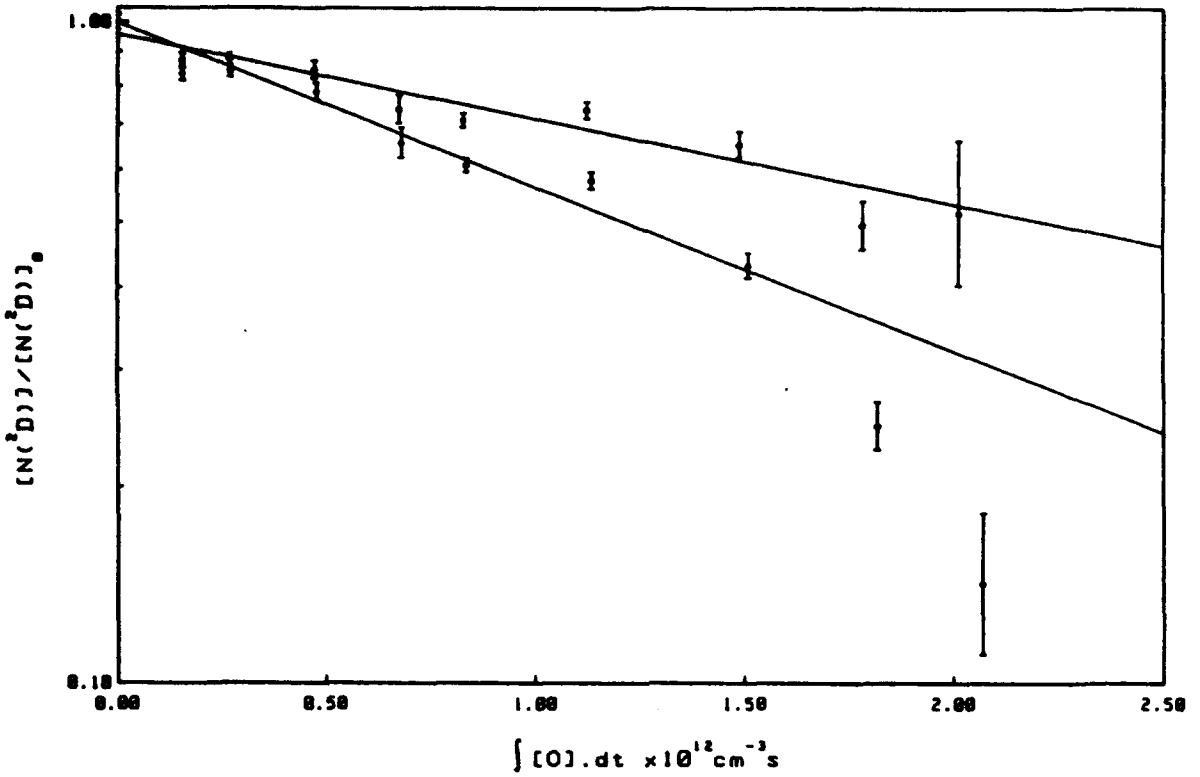

FIG. 9. Upper and lower bounds to $N(^2D)$ decay as a function of $\int_0^t [O]dt$ for the data shown in Fig. 7. Lower trace: $k_N = 4.3\times10^{-11}$ cm^3 s^{-1}, $k_{NO} = 8.06\times10^{-11}$ cm^3 s^{-1} and $[N(^4S)] = 3.44$ mTorr. Upper trace: $k_N = 2.5\times10^{-11}$ cm^3 s^{-1}, $k_{NO} = 5.49\times10^{-11}$ cm^3 s^{-1} and $[N(^4S)] = 3.12$ mTorr.

pected to be short compared to the flowtime. Given the long flowtime and large $N(^4S)$ concentration, $\int_0^t [O]dt \rightarrow [NO]_0 t$ and the correction for the NO contribution to the decay involves primarily a y-axis adjustment. The magnitude of this adjustment is sensitive to the exact values used for k_N and k_{NO}. In the interests of self-consistency within the analysis, when one extreme value of k_N was taken in the error calculation, the value of k_{NO} calculated using that same value was used. Thus the k_N and k_{NO} errors are correlated and, in this instance, tend to cancel one another. The measurement of k_O is therefore less sensitive to the uncertainty in k_N than is k_{NO}. The error bounds for k_O were calculated using the extreme values of $[N(^4S)]$, k_N, and k_{NO}. The results are shown in Figs. 9 and 10 for the data in Figs. 7 and 8, respectively. The results of twelve separate kinetic runs are given in Table II. As before, the errors quoted for each value are the statistical values in each limit and are small compared to the uncertainties arising from the correlated systematic errors. The weighted averages of these data give a value for k_O of $(6.93 + 0.71, -1.08)\times10^{-13}$ cm^3 s^{-1}. The absence of any systematic variation in k_O with t confirms that there is no significant loss of $O(^3P)$ along the flow tube. The O_2 formed would react rapidly with $N(^2D)$, giving an apparent increase in k_O at longer reaction times.

V. CONCLUSIONS

The previously reported experimental and modeling values of k_O are listed in Table III. The value of k_O reported here is in good agreement with the most recent experimental measurement made by Piper,[32] who utilized $O(^3P)$ atom generation and $N(^2D)$ detection techniques differing from those employed here. It is also in fair agreement with the earlier results of Davenport *et al.*[33] and Ianuzzi *et al.*[9] The major conflict is with the result of Jusinski *et al.*,[11] who recently rekindled the ongoing controversy regarding the disparity between experimental measurements and the preferred modeling values by suggesting that the true rate was of the order of 2.1×10^{-11} cm^3 s^{-1}. The experiment by Jusinski *et al.* and the studies reported here were performed using an essentially identical experimental setup and methodology. The origin of the disparity in the results is not immediately apparent although it is interesting to note that our preliminary investigations (as illustrated in Fig. 2) also yield a value of $k_{eff} \sim 2\times10^{-11}$ cm^3 s^{-1} at $t = 7.5$ ms. Our results and calculations indicate that, for the conditions reported in Ref. 11 ($[N(^4S)] = 10$ mTorr, $t = 7.5$ ms), an effective rate constant (which is what was actually reported) of $\sim2\times10^{-12}$ cm^3 s^{-1} should be observed. The order of magnitude difference cannot be accounted for by any reasonable

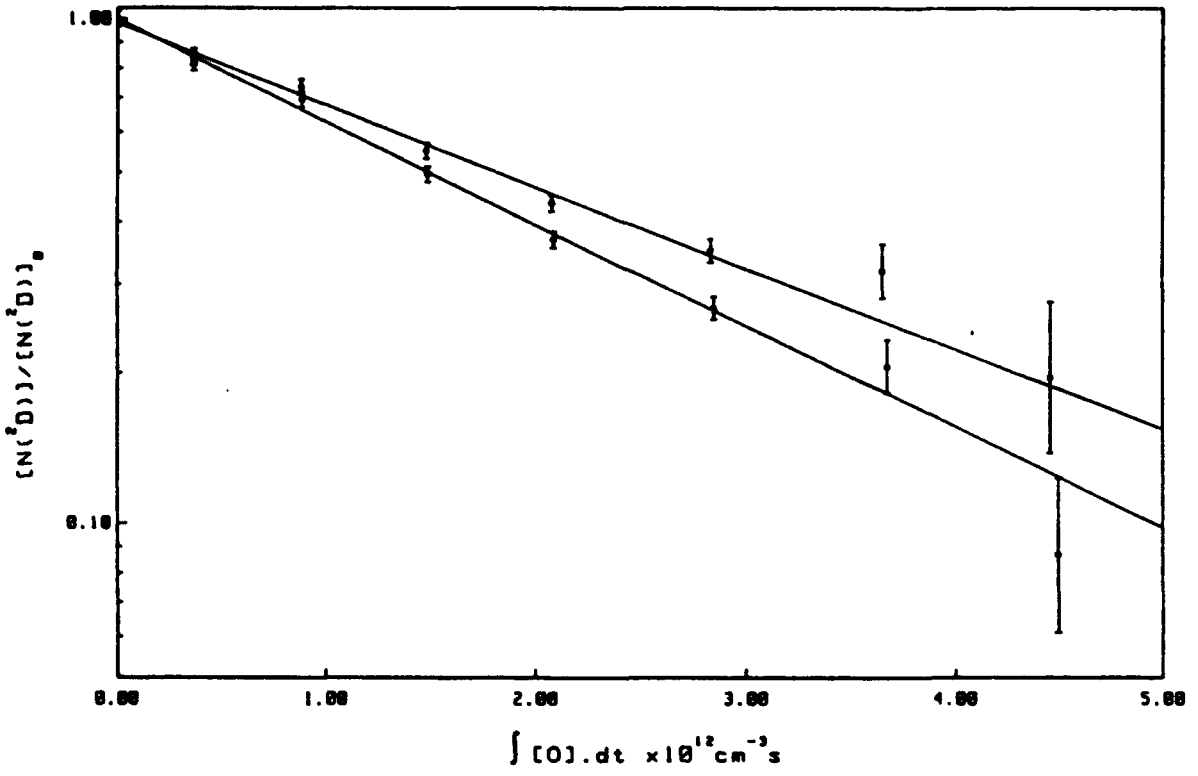

FIG. 10. Upper and lower bounds for $N(^2D)$ decay as a function of $\int_0^t [O]dt$ for the data shown in Fig. 8. Lower trace: $k_N = 4.3\times10^{-11}$ cm^{3}s^{-1}, $k_{NO} = 8.06\times10^{-11}$ cm^{3}s^{-1} and $[N(^4S)] = 4.49$ mTorr. Upper trace: $k_N = 2.5\times10^{-11}$ cm^{3}s^{-1}, $k_{NO} = 5.49\times10^{-11}$ cm^{3}s^{-1}, and $[N(^4S)] = 4.01$ mTorr.

adjustment for poor mixing. It is possible that the faster rate observed is the result of the quenching of some precursor which is the dominant $N(^2D)$ source in their higher pressure system ($\sim$30 Torr). The nonlinearity observed in some of their plots would tend to support this hypothesis.

TABLE II. Kinetic data for determination of $N(^2D) + O(^3P)$ rate coefficient.

	k_o, cm^3 molecule^{-1} s$^{-1}\times10^{-13}$		
t, ms	Lower bound[a]	Mid range[b]	Upper bound[c]
23	4.74 ± 0.37	7.60 ± 0.37	9.17 ± 0.37
	3.37 ± 0.50	6.38 ± 0.49	8.03 ± 0.49
31.7	5.33 ± 0.23	6.81 ± 0.23	7.57 ± 0.23
	5.08 ± 0.31	6.78 ± 0.31	7.64 ± 0.31
36.1	7.12 ± 0.26	8.51 ± 0.26	9.27 ± 0.26
	6.01 ± 0.24	7.44 ± 0.24	8.27 ± 0.24
41.4	6.62 ± 0.21	7.58 ± 0.21	8.14 ± 0.21
	6.01 ± 0.26	6.99 ± 0.26	7.53 ± 0.26
44.8	5.46 ± 0.28	6.21 ± 0.27	6.63 ± 0.27
	5.32 ± 0.28	6.09 ± 0.28	6.52 ± 0.28
55	6.19 ± 0.17	6.65 ± 0.17	6.90 ± 0.17
	5.54 ± 0.23	6.05 ± 0.23	6.33 ± 0.23
Weighted mean	5.85 ± 0.08	6.93 ± 0.08	7.64 ± 0.08

[a] Using $k_N = 2.5\times10^{-11}$ cm^{3}s^{-1}, $k_{NO} = 5.49\times10^{-11}$ cm^{3}s^{-1}.
[b] Using $k_N = 3.4\times10^{-11}$ cm^{3}s^{-1}, $k_{NO} = 6.70\times10^{-11}$ cm^{3}s^{-1}.
[c] Using $k_N = 4.3\times10^{-11}$ cm^{3}s^{-1}, $k_{NO} = 8.06\times10^{-11}$ cm^{3}s^{-1}.

The method of generating $O(^3P)$ atoms necessarily means that NO molecules will be present in the flow for some finite time. As k_{NO} turns out to be nearly 2 orders of magnitude larger than k_O, this will always be significant although, by carefully controlling the experimental conditions, the NO contribution can be kept to a minimum. It is essential that the flow conditions be precisely characterized for each kinetic run, and that the analysis carried out with extreme care, if meaningful results are to be recovered. This also applies to the NO results. In this instance, the requirement that the measurements be carried out at very short reaction times brings us to the limits of flow tube technology. The mixing time, using standard injectors and flows, becomes a significant fraction of the total flow time and must be carefully considered to avoid reporting artificially low values. The accuracy of the reported value of k_{NO} is primarily dictated by the confidence limits associated with k_N. Should a more precise value of k_N become available, the confidence limits on k_{NO} may be reduced accordingly.

Experimental measurements of k_O encounter a number of difficulties, the most immediate of which are, the generation of a pure source of $O(^3P)$ atoms, their transportation to the reaction zone and the subsequent efficient mixing of the reactants. The method of titrating NO directly into the flow tube ingeniously solves the transportation and mixing difficulties but introduces an additional complication as the $O(^3P)$ precursor itself is a highly reactive impurity. With

TABLE III. Experimental and a representative sample of modeling determinations of k_o.

	k_o, $cm^3 s^{-1}$	Source	Reference
Experimental	$(1.8 \pm 0.6) \times 10^{-12}$	Davenport *et al.* (1976)	33
	$< 1.8 \times 10^{-12}$	Ianuzzi and Kaufman (1980)	9
	$(2.1 \pm 0.8) \times 10^{-11}$	Jusinski *et al.* (1988)	11
	$(1.06 \pm 0.26) \times 10^{-12}$	Piper (1988)	32
	$(6.9 \pm 1.0) \times 10^{-11}$	This work	
Modeling	1×10^{-12}	Strobel *et al.* (1970)	2
	$< 10^{-14}$	Oran *et al.* (1975)	12
	4×10^{-13}	Frederick and Rusch (1977)	13
	1×10^{-12}	Cravens *et al.* (1979)	14
	4×10^{-13}	Rusch and Gerard (1980)	15
	6×10^{-13}	Richards *et al.* (1981)	36
	$\sim 1 \times 10^{-12}$	Fesen *et al.* (1989)	35

precise characterization of flow conditions and careful analysis of results, an accurate value for k_O can be recovered.

Recent models for atmospheric NO concentrations have tended to favor larger values of k_O, and it would appear that experiment and theory have finally reached a consensus regarding the preferred value of this rate coefficient. Bates[34] has shown that the fast rate coefficient reported by Jusinski *et al.*[11] is incompatible with observed data on OI red line emission at 630 nm. Also, the most recent modeling calculation by Fesen[35] successfully accounts for observed NO distributions using a value of $k_O = 1 \times 10^{-12}$ $cm^3 s^{-1}$, which coincides with the most recent experimental determinations.

ACKNOWLEDGMENTS

This research was performed under Contract No. F19628-86-C-0139 from the Air Force Geophysics Laboratory, and sponsored by the Air Force Office of Scientific Research under Task 2310G4. We thank Dr. Tom G. Slanger (SRI International) and Dr. Larry Piper (Physical Sciences, Inc.) for very useful discussions.

[1] R. B. Norton and C. A. Barth, J. Geophys. Res. 65, 1469 (1970).
[2] D. F. Strobel, D. N. Hunten, and M. B. McElroy, J. Geophys. Res. 75, 4307 (1970).
[3] D. W. Rusch, J. Geophys. Res. 78, 5676 (1973).
[4] C. A. Barth, J. Geophys. Res. 69, 3301 (1964).
[5] L. G. Piper, M. E. Donahue, and W. T. Rawlins, J. Phys. Chem. 91, 3883 (1987).
[6] C.-L. Lin and F. Kaufman, J. Chem. Phys. 55, 3760 (1971).
[7] T. G. Slanger, B. J. Wood, and G. Black, J. Geophys. Res. 76, 8430 (1971).
[8] G. Black, T. G. Slanger, G. A. St. John, and R. A. Young, J. Chem. Phys. 51, 116 (1969).
[9] M. P. Ianuzzi and F. Kaufman, J. Chem. Phys. 73, 4701 (1980).
[10] B. Fell, I. V. Riva, and D. L. McFadden, J. Phys. Chem. 85, 224 (1981).
[11] L. E. Jusinski, G. Black, and T. G. Slanger, J. Phys. Chem. 92, 5977 (1988).
[12] E. S. Oran, P. S. Julienne, and P. F. Strobel, J. Geophys. Res. 80, 3068 (1975).
[13] J. E. Frederick and D. W. Rusch, J. Geophys. Res. 82, 3509 (1977).
[14] T. E. Cravens, J. C. Gerard, A. I. Stewart, and D. W. Rusch, J. Geophys. Res. 84, 2675 (1979).
[15] D. W. Rusch and J. C. Gerard, J. Geophys. Res. 85, 1285 (1980).
[16] I. C. Winkler, R. A. Stachnik, J. I. Steinfeld, and S. M. Miller, J. Chem. Phys. 85, 890 (1986).
[17] D. Hussain, S. K. Mitra, and A. N. Young, J. Chem. Soc. Faraday Trans. 2 70, 1721 (1974).
[18] G. Black and L. E. Jusinski, Chem. Phys. Lett. 139, 41 (1987).
[19] C. M. Phillips, J. I. Steinfeld, and S. M. Miller, J. Phys. Chem. 91, 5001, (1987).
[20] C. E. Moore, Atomic Energy Levels, Vol. I, NSRDS-NBS35, U.S. (Government Printing Office, Washington, D.C., 1971).
[21] J. H. Lee, J. V. Michael, W. A. Payne, and L. Steif, J. Chem. Phys. 69, 3069 (1978).
[22] J. E. Morgan and H. F. Schiff, Can J. Chem. 42, 2300 (1964).
[23] G. Black and T. G. Slanger, J. Chem. Phys. 74, 6517 (1981).
[24] H. Zacharias, M. M. T. Loy, P. A. Roland, and Aa. S. Sudbo, J. Chem. Phys. 81, 3148 (1984).
[25] I. C. Winkler, R. Stachnik, J. I. Steinfeld, and S. M. Miller, Spectrochim. Acta A 42, 339 (1986).
[26] L. E. Jusinski, G. E. Gadd, G. Black, and T. G. Slanger, J. Chem. Phys. 90, 4282 (1982).
[27] G. E. Gadd, L. E. Jusinski, and T. G. Slanger, J. Chem. Phys. 91, 3378 (1989).
[28] H. C. Yang and T. M. Niemczyk, Anal. Chem. 58, 2492 (1986).
[29] L. G. Piper, Report No. PSI-050-TR-509 (Physical Sciences Inc., Wakefield, Mass., 1985).
[30] L. G. Piper, L. M. Cowles, and W. T. Rawlins, J. Chem. Phys. 85, 3369 (1986).
[31] R. A. Young, R. L. Sharpless, and R. Stringham, J. Chem. Phys. 40, 117 (1964).
[32] L. G. Piper, J. Chem. Phys. 91, 3516 (1989).
[33] J. E. Davenport, T. G. Slanger, and G. Black, J. Geophys. Res. 81, 12 (1976).
[34] D. R. Bates, Planet Space Sci. 37, 1145 (1989).
[35] C. G. Fesen, J. C. Gerard, and D. W. Rusch, J. Geophys. Res. 94, 5419 (1989).
[36] P. G. Richards, D. G. Torr, and M. R. Torr, J. Geophys. Res. 86, 1495 (1981).

RESEARCH NOTE

DETECTION OF N(^{4}S) BY RESONANTLY ENHANCED MULTIPHOTON IONIZATION SPECTROSCOPY

(Received 1 December 1989)

Abstract - We report the first instance of detection of N(^{4}S) atoms by Resonantly Enhanced Multiphoton Ionization (REMPI). The magnitude of the ion signal, after correction for laser power dependence, is directly proportional to the N(^{4}S) concentration and, once calibrated, is a direct and highly sensitive method for N(^{4}S) concentration measurements in fast-flow kinetics experiments.

INTRODUCTION

In experiments utilizing active nitrogen flows, it is generally necessary to know the ground state nitrogen atom concentration. This value is usually determined using a standard NO titration technique [1]. This method makes use of the reactions

$$N(^4S) + NO \rightarrow N_2 + O(^3P) \qquad (1)$$

and

$$NO + O + M \rightarrow NO_2^* + M \qquad (2)$$

Reaction (1) is rapid [2] and serves to deplete [N(^{4}S)] stoichiometrically. Monitoring the N_2 first positive emission around 580nm gives a fluorescence signal proportional to [N(^{4}S)]^2 for [NO]<[N(^{4}S)]. Beyond the end point NO_2^* emission following reaction (2) gives a signal proportional to NO in the same spectral range. This technique works well provided that reaction (1) has sufficient time to go to completion and N(^{4}S) is present in sufficient quantity. If this is not the case then both the N_2 first positive and NO_2^* emission will contribute to the signal level.

Many reactions involving metastable atoms and molecules require fast flow conditions due to the rapid decay of the metastable concentration. The reactions

$$N(^2D) + NO \rightarrow N_2 + O \qquad (3)$$

and

$$N(^2P) + O_2 \rightarrow NO + O \qquad (4)$$

are examples of this [3-5]. In order to calculate the rate coefficient of reaction (3), [N(^{4}S)] must be known in order to determine the rate of depletion of NO via reaction (1). Under certain conditions, the flow time and N(^{4}S) concentration may be such that reaction (1) does not go to completion and the standard NO titration technique will no longer give accurate values for [N(^{4}S)]. The use of Resonantly Enhanced Multiphoton Ionization (REMPI) to measure relative N(^{2}D) and N(^{2}P) concentrations is well established [5,6]. Here we report, to our knowledge, the first instance of REMPI detection of N(^{4}S) atoms. The magnitude of the ion signal is directly proportional to the N(^{4}S) concentration and, once calibrated, may be used to measure N(^{4}S) absolutely.

EXPERIMENTAL

These investigations were carried out using the FACELIF afterglow reactor which has been described in detail elsewhere [4,7]. A schematic of the experimental apparatus is shown in Fig. 1. The N(^{4}S) atoms are generated in a flow of 1-2% N_2 in He, using a microwave discharge. The current created by the photoions, across a pair of Ni wire grids, biased at 90V, is amplified using an *Ithaco model 1211 current amplifier* and detected on an EG & G model 162 Boxcar Averager. The laser power is also monitored using a Molectron Pyroelectric joulemeter (J3-09). The fluorescence measurements are made using a photomultiplier tube through a 580 ± 5 nm filter. The NO used for these titrations is a 5% mixture of NO in He and is added through a loop injector upstream of the detection region. Typical flow times were 25-30ms with total tube pressures of 2.5-3.5 Torr. These slow flow/high pressure conditions are best suited to making NO titration measurements of [N(^{4}S)] giving comparatively intense signals and allowing reaction (1) ample time to go to completion. The N(^{4}S) concentration could be varied either by adjusting the N_2 to He ratio (this was typically 1-3% N_2 in He) or more conveniently by altering the microwave power.

The transition N($2p^2 3p\ ^4D_J^0$) ← N($2p^3\ ^4S_{3/2}^0$) may be resonantly excited by two 211 nm photons [8], and the atom then ionized by a third photon of the same energy. Laser radiation at 211 nm may be generated by stimulated Raman frequency shifting of the doubled output of a Nd:YAG pumped dye laser [9] but this generally gives pulse energies of less than 100 mJ. Significantly higher pulse energies are desirable for REMPI detection. Here we have used a BBO crystal to double the output from a Nd:YAG pumped dye laser (Quanta-Ray DGR2A, PDL-1, INRAD Autotracker II) directly. Stilbene 420 laser dye gave pulse energies of approximately 0.5 mJ, measured after exiting the flow tube.

This power level decreased rapidly in time with the dye having a useful lifetime of about 20 minutes. The decrease proved advantageous when taking measurements of the power dependence of the ion signals, enabling a large number of data points to be taken without the extensive use of neutral density filters to attenuate the beam. When making quantitative measurements of [N(^{4}S)], however, it is desirable to keep the laser power as constant as possible to minimize corrections necessary for power normalization of ion signals. We found that the use of ~ four times larger dye reservoirs greatly enhanced the useful life of the dye and also minimized power variations during the course of data acquisition.

ABSOLUTE [N(^{4}S)] MEASUREMENTS

The N(^{4}D$_J^0$) state is split into four levels, J=1/2, 3/2, 5/2, and 7/2, at 94770.85, 94793.46, 94830.86, and 94881.79 cm^{-1}, respectively. The relative intensities are simply given by the upper state degeneracy (2J+1) and the observed spectrum will be a quartet with intensity ratios of 1:2:3:4 (J=1/2:3/2:5/2:7/2). The observed spectrum is shown in Fig. 2. The most intense line was used throughout for all quantitative measurements of [N(^{4}S)]. To normalize the signal levels accurately for variations in laser power, it was necessary to characterize the power dependence of the ion signal precisely prior to any data acquisition. The ion signal is proportional to some power N of the laser intensity I, and therefore a plot of ln (ion signal) vs. ln I will have a slope equal to N. The results of doing this are shown in Fig. 3. The slope varies between 2.8 and 1.5 going from low to higher power. This indicates that the two photon transition is becoming saturated at the higher powers. A similar power dependence was observed for (2+1) photon ionization of N(^{2}D) at 269nm [10], although somewhat different conclusions were drawn in that work regarding the relative saturation of the excitation and ionization steps. The two photon excitation cross-section for this transition has been calculated [9] and therefore the transition rate may be calculated. The fit of the data in Fig. 3 is obtained using a simple rate equation model for a three level system [11]. Strictly speaking, correct normalization of signals for power variations requires that signal and laser power be recorded for each pulse [12]. Here we have recorded the average ion signal and laser power over a large number of pulses with the beam tightly focused between the detector grids. The resulting ion signal therefore consists of contributions over a range of saturation conditions. It is thus inappropriate to comment on the magnitudes of the experimentally observed rates for either the ionization or the two photon excitation. For the purposes of this study it is only necessary to be able to understand the bulk behavior of the system. Fig. 3 indicates that for small variations in average laser power (±5%) it is a reasonable approximation to use the same laser power dependence factor when normalizing the ion signals.

For conditions where reaction (1) has time to go to completion, [N(^{4}S)] may be determined by observing the reduction in the ion signal as NO is added. The x-axis intercept on a plot of the ion signal vs. [NO] gives the value of [N(^{4}S)]. The slope of this line serves to calibrate the ion signal level in terms of absolute [N(^{4}S)] concentrations. In order to verify the accuracy of this technique for [N(^{4}S)] measurement, comparative measurements were taken using REMPI and the standard fluorescence monitoring titration technique [1]. The results are listed in Table 1. The REMPI results are the x-axis intercept of a weighted linear regression fit of NO titration data sets with ±2σ error limits. The standard titration measurements may be considered accurate to ±5%. The results are in good agreement indicating that the REMPI technique yields accurate values for [N(^{4}S)].

DISCUSSION

REMPI provides a sensitive method for quantitatively detecting ground state nitrogen atoms. Number densities on the order of 10^{10} atoms cm^{-3} were easily detected compared to a limit, for our flow system, of around 2×10^{13} atoms cm^{-3} using the more usual titration technique. Below this level the fluorescence measurements encountered problems in the form of stray light from the discharge reaching the detector. A more serious problem can arise from fluorescence due to sources other than N(^{4}S) atom recombination, which contributes significantly to the signal intensity [4,13]. Unlike the standard technique, REMPI offers a state specific method of monitoring [N(^{4}S)] directly and is therefore less susceptible to extraneous signals. The signal level may be calibrated under slow flow/high [N(^{4}S)] conditions. The magnitude of the ion signal may then be used to give a direct measurement of [N(^{4}S)] for experiments requiring fast flows where [N(^{4}S)] may be low; these condition are inappropriate for standard titration measurements.

Acknowledgments: This research was performed under contract F19628-86-C-0139 from the Air Force Geophysics Laboratory, and sponsored by the Air Force Office of Scientific Research under Task 2310G4.

Department of Chemistry, Massachusetts Institute of Technology, Cambridge, Massachusetts 02139, U.S.A.
C.P. FELL
J.I. STEINFELD

Air Force Geophysics Laboratory, Hanscom Air Force Base Bedford, Massachusetts 01731, U.S.A.
S.M. MILLER

REFERENCES

[1] F. Kaufman and J.R. Kelson, *7th International Symposium on Combustion* (Oxford University, Oxford, 1958), p 53.

[2] J.H. Lee, J.V. Michael, W.A. Payne and L.J. Steif, J. Chem. Phys. 69, 3069 (1978).

[3] C.-L. Lin and F. Kaufman, J. Chem. Phys. 55, 3760 (1971).

[4] C.P. Fell, J.I. Steinfeld, and S.M. Miller, J. Chem. Phys., in press.

[5] C.M. Phillips, J.I. Steinfeld and S.M. Miller, J. Phys. Chem. 91, 500 (1987).

[6] G. Black and L.E. Jusinski, Chem. Phys. Lett. 139, 41 (1987).

[7] I.C. Winkler, R.A. Stachnik, J.I. Steinfeld and S.M. Miller, J. Chem. Phys. 85, 890 (1986).

[8] C.E. Moore, *Atomic Energy Levels*; NSRDS-NBS35, Vol. I; U.S. Government Printing Office: Washington, D.C., (1971).

[9] W.K. Bischel, B.E. Perry and D.R. Crosley, Appl. Opt. 21, 1419 (1982).

[10] L.E. Jusinski, G.E. Gadd, G. Black and T.G. Slanger, J. Chem. Phys. 90, 4282 (1989).

[11] J.I. Steinfeld, J. Klaassen, and C.P. Fell (to be published).

[12] C. Jacobs, R.J. Madix and R.N. Zare, J. Chem. Phys., 85, 5469 (1986).

[13] L.G. Piper, Report No. PSI-050-TR-509 (Physical Sciences Inc., Wakefield, Mass., 1985).

Table 1. Comparison of [N(^{4}S)] titrations by NO using standard chemiluminescence detection and direct MPI detection under flow conditions. [N(^{4}S)] given in mTorr.

Standard NO Titration	MPI-Titration
4.38	4.48 ± 0.18
3.28	3.40 ± 0.10
2.65	2.50 ± 0.14
2.02	1.96 ± 0.12
1.97	1.97 ± 0.12
1.42	1.51 ± 0.07

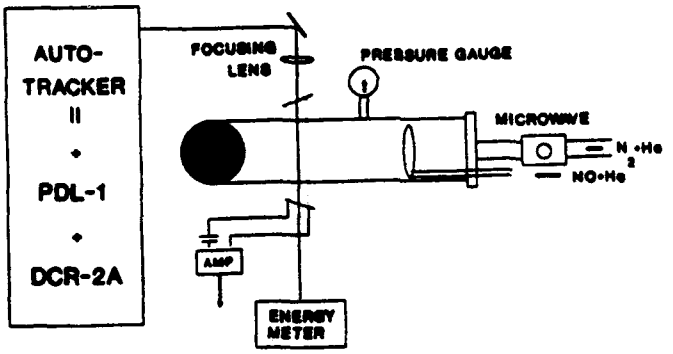

FIG. 1. Schematic of FACELIF experimental apparatus. The solid circle represents a right angle connection to the pumping system.

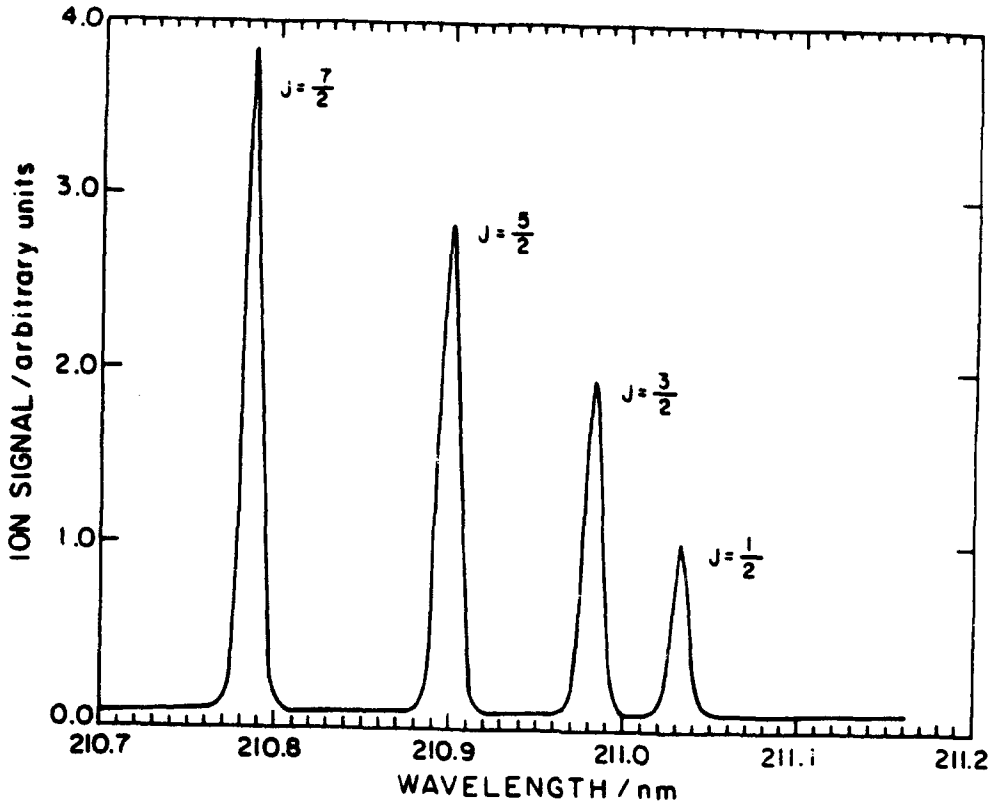

FIG. 2. Three photon (two to resonance) ionization spectrum of $N(^4S_J)$.

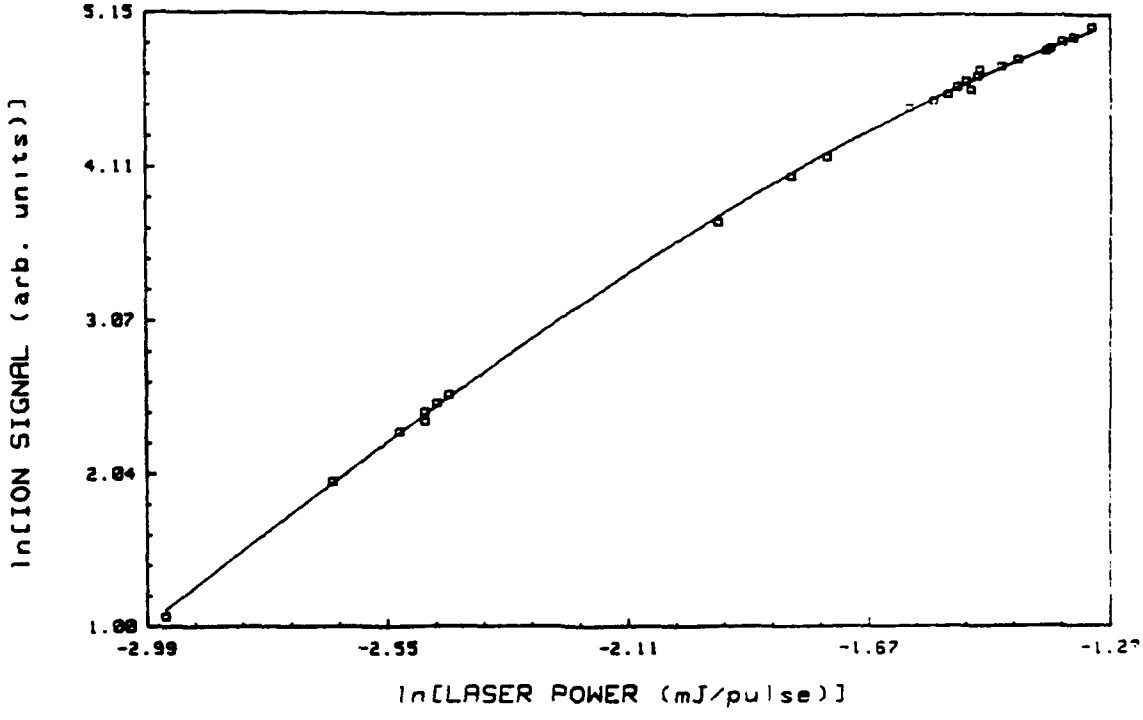

FIG. 3. Power dependence of $N(^4S)$ ionization signal.